Degree Day

BuildForward™

Future Climate Design Criteria for Architects and

BERGSTROM AFB/AUSTIN INTL

Austin, Texas (Travis County (United States of America)

Prepared For:

[Company]
Street Address, State,
City Postal Code, Country

Prepared By:

Degree Day LLC
degreeday.org
info@degreeday.org

Revisions

Rev	Description	Date
Version 1.0	Initial Release	01.14.2025

PROFESSIONAL USE DISCLAIMER

The information and climate projections presented herein are provided to support planning-level, screening, and risk-informed decision-making and do not constitute predictions, forecasts, or guarantees of future conditions. These results are not intended to replace site-specific investigations, detailed engineering analyses, or the services of a licensed professional.

When used to inform design or engineering decisions, the outputs should be interpreted in conjunction with applicable codes, standards, regulatory requirements, and professional judgment. Additional analysis may be required to determine suitability for project-specific or code-compliance applications.

The data and methods employed are intended to produce scientifically defensible results; however, inherent uncertainties remain due to model formulation, spatial resolution, parameterization of physical processes, and limitations in representing localized hazards.

The analyses reflect the state of scientific knowledge at the time of publication and may evolve as new data, models, and technical guidance become available. Users are responsible for evaluating the fitness of the information for their intended purpose and for supplementing these results with observed data, alternative analytical approaches, and applicable design standards as appropriate.

Executive Summary

Cooling Design Conditions Already Exceed Historical Assumptions

Observed records show statistically significant increases in cooling-relevant metrics:

- Individual heatwave events last 24% longer per decade
- Very hot days (≥95°F): +18% per decade
- Cooling Degree Days (CDD65): +5.3% per decade

Engineering Implication:

Historical cooling design values increasingly underrepresent current operating conditions.

Cooling Load Growth Accelerates Under Future Conditions

- CDD65 increases ~18% by 2050, ~39% by 2080
- Historical 100-year heat events occur every 10–20 years by late century
- Dry-bulb design temperatures increase modestly, but extreme heat frequency shifts materially

Engineering Implication:

System sizing based on historical exceedance criteria will result in increased hours at or beyond design capacity.

Historical Heating Design Remains Conservative

Cold extremes have not warmed as much as hot extremes.

Engineering Implication:

Historical heating design temperatures remain appropriate, particularly for freeze protection and life-safety systems.

Exposure to Severe Thunderstorms and Large, Damaging Hail is High

The site is currently 98th percentile nationally for thunderstorm intensity and 85th percentile for large hail frequency (≥1 inch). Future conditions cannot be reliably estimated given current scientific understanding.

Engineering Implication:

Impact-rated materials, protected glazing, and shielding of exposed mechanical, electrical, and PV systems are warranted under current conditions.

Table of Contents

1 How to use this report

Climate change is making historical weather records increasingly inadequate for informing facility-related design decisions. Traditionally, local weather station data has been used to estimate thermal loads, optimize occupant comfort, size site drainage, forecast energy use, and more. However, to ensure that building systems and infrastructure perform reliably over their full design life, it is now prudent to consider how climate conditions are expected to change over the course of a facility's service life.

While historical weather observations are widely available, future climate projections at the scale of individual weather stations are generally not.

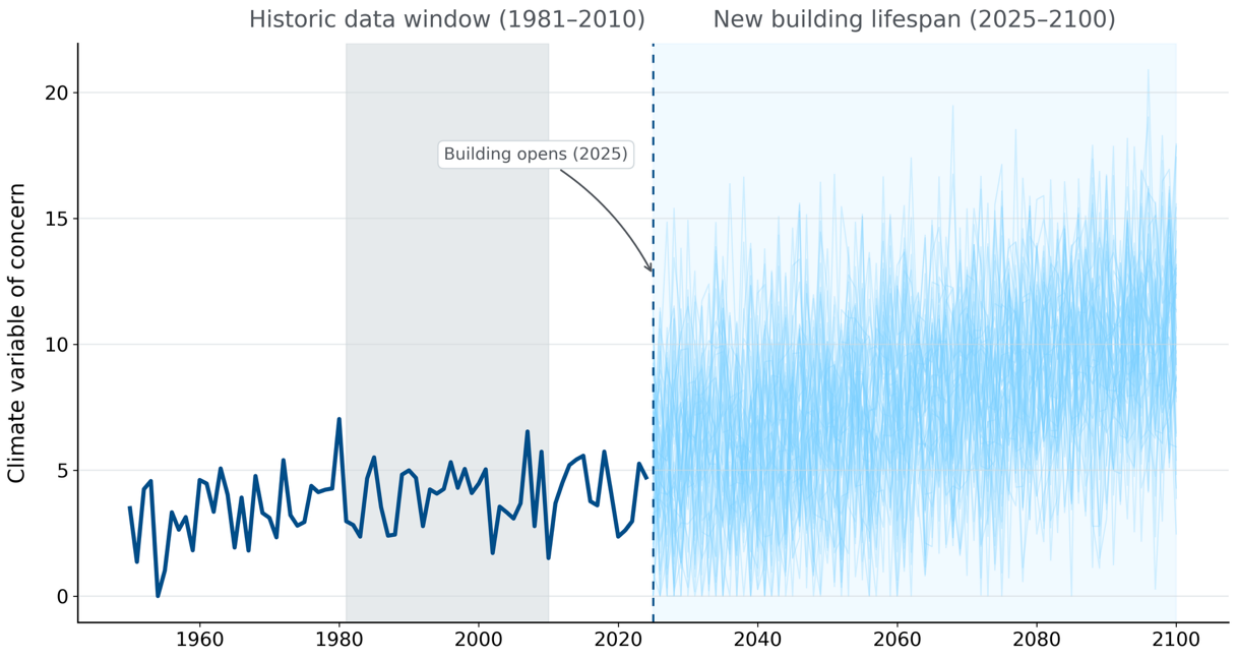

Figure 1 Illustrative example of a hypothetical climate variable showing changes in frequency and intensity relative to a historical baseline (1981–2010) over the intended service life of a new building (2025–2100). The dashed line marks the start of operations.

1.1 Purpose and Scope

This report presents curated weather, climate, and natural hazard information to support facility planning and design decisions, including considerations related to equipment sizing, foundation depth, material selection, and building energy modeling. The projections provide a scientifically credible evidence base to support informed, risk-aware decision-making by design teams and asset owners. Future climate projections are derived from station-calibrated climate data that better captures local conditions and extreme events compared to standard gridded climate products.

The data serve two primary functions:

1. Augmenting existing design standards that are based on historical conditions and do not explicitly account for future climate change
2. Filling information gaps where authoritative sources, regulatory guidance, or long-term weather station records are unavailable or incomplete

The projections are intended to inform professional engineering judgment and to supplement authoritative design standards, codes, and guidance. They are not a substitute for governing codes, regulations, or jurisdictional requirements, which remain controlling.

Where authoritative climate or hazard guidance is unavailable, incomplete, or not forward-looking, the data may provide additional context for evaluating potential future conditions over an asset's service life, supporting risk-informed planning and design discussions.

1.2 Future Warming Pathway

This report provides weather-station-calibrated climate projections for two planning horizons: mid-century (2050) and late-century (2080). Projections are based on a 3°C global warming scenario—a middle-range climate future consistent with current emissions trends and expert assessments of likely 21st-century warming.

For context, global temperatures have already warmed 1.3-1.4°C above pre-industrial levels (1850-1900) as of 2025. Under the 3°C scenario, warming reaches approximately 2°C by mid-century and 3°C by 2080. This warming translates to specific changes in local temperature extremes, precipitation patterns, and wind speeds at your project location, detailed in the sections below.

Technical Note: In climate modeling terminology, this scenario falls between SSP2-4.5 and SSP3-7.0 pathways and is well below high-end SSP5-8.5 outcomes. No familiarity with these labels is required to use this report.

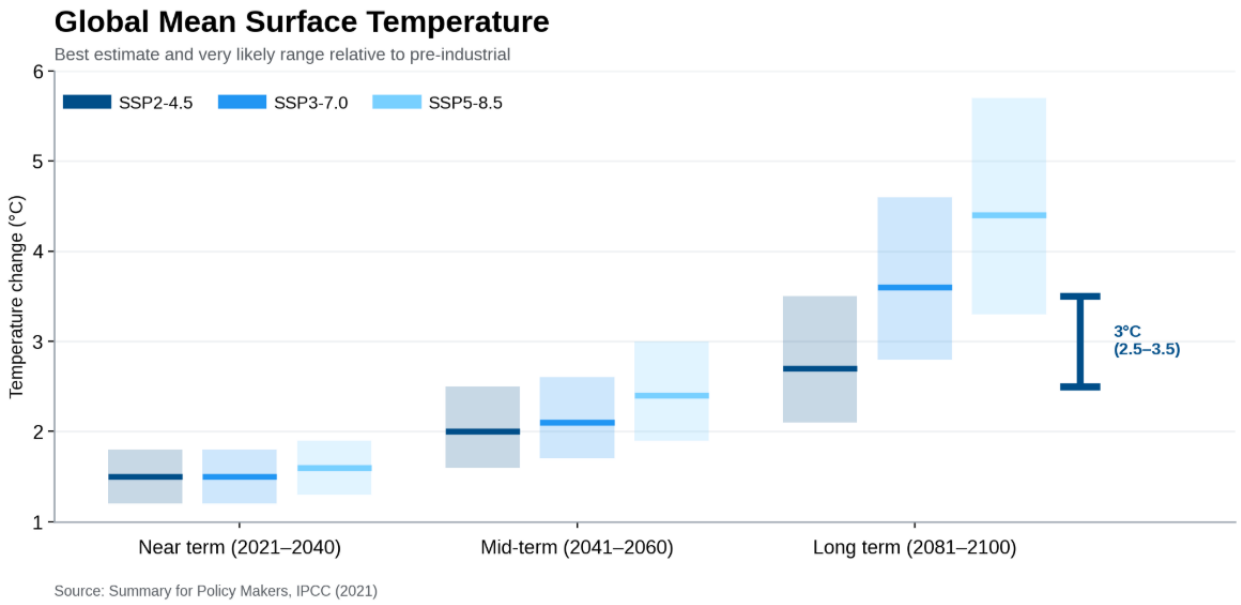

Figure 2 Projected global mean surface temperature change relative to pre-industrial levels (1850–1900) across near-, mid-, and long-term periods under selected emissions pathways. The 3 °C global mean surface temperature level is used as a reference threshold in this report.

1.3 Design Horizon Selection

Selection of an appropriate time horizon should consider asset lifespan, replaceability, and adaptability, recognizing that different components within a system may warrant different planning horizons.

Late-century (2080) projections are recommended for permanent or long-lived infrastructure elements (beyond 30 years), where future climate conditions may differ materially from historical conditions. This includes:

- Foundation depth and types
- Structural load-bearing capacity
- Site drainage sizing and grading
- Finish floor elevations
- Components that are difficult or costly to modify once constructed, where future changes would be disruptive or uneconomical

Using late-century information can also help contextualize long-term exposure and potential future constraints, particularly where redesign options are limited. For example, permanent inundation from sea-level rise or regular high tide flooding.

Mid-century (2050) projections are recommended for equipment and systems with defined replacement or upgrade cycles (approximately 15–30 years), including:

- HVAC systems and chillers
- Refrigeration systems
- Electrical transformers and switchgear
- Back-up generators
- Solar Photovoltaic (PV) panels
- Other systems or components designed with planned flexibility, where future adaptation or replacement is feasible

For these elements, mid-century projections provide insight into conditions likely to be encountered within a typical design or planning horizon.

Critical and high-consequence facilities

For facilities where service continuity and reliability are essential, such as hospitals, data centers, emergency services, and critical utility infrastructure, engineers may wish to review both mid- and late-century projections to better understand a broader range of potential future conditions and to support risk-informed decision-making.

1.4 When to seek additional analysis

Additional project-specific analysis should be considered where decisions are highly sensitive to localized conditions or high-consequence failure modes. This includes, but is not limited to, applications involving critical infrastructure, life-safety considerations, or assets with service lives extending well beyond mid-century. Further analysis may also be warranted where hazards are strongly influenced by local topography (e.g., site grading), land use, microclimate effects, or compound hazard processes—such as convective storms, flooding mechanisms, or wildfire behavior—that are not fully resolved by the methods used herein. In such cases, users are encouraged to supplement the information presented with site-specific measurements (including surveying and private weather station records), higher-resolution or alternative modeling approaches, local knowledge, sensitivity analyses, or consultation with qualified subject-matter experts to ensure fitness for purpose.

2 Site Context and Overview

2.1 Location

Travis County is in South Central Texas. The region features a Humid Subtropical climate (Köppen *Cfa*) characterized by long, hot summers and mild winters. Situated in the path of both continental air masses and moisture plumes from the Gulf of Mexico, the county experiences highly variable weather patterns, ranging from extended droughts to intense convective precipitation.

2.1.1 Elevation

Travis County exhibits a strong west–east elevation gradient, with rugged, high-relief Hill Country terrain in the west transitioning to lower, flatter plains in the east. The Colorado River and its reservoir system (including Lake Travis and Lake Austin) form the dominant hydrologic feature, carving through the county and widening into floodplains toward the east. The Austin–Bergstrom area is located on relatively low, gently sloping terrain adjacent to the river system, contrasting with the steeper uplands to the west.

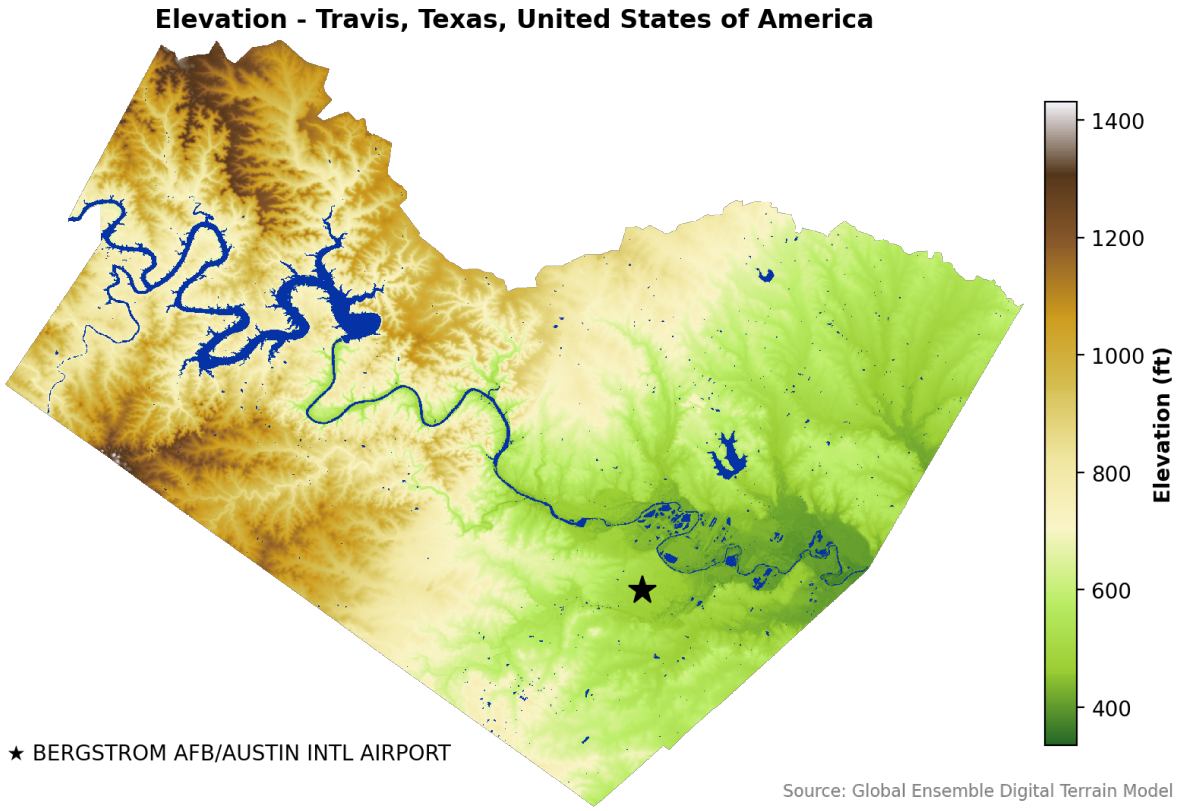

Figure 3 Elevation and major watercourse features of Travis County, Texas, with the location of Austin–Bergstrom International Airport indicated. Elevation shown in feet above mean sea level.

2.1.2 Land Use and Land Cover

Land cover in Travis County is dominated by forest and dense vegetation, particularly in the western Hill Country, reflecting more rugged terrain and natural cover. Urban land cover is concentrated in the central corridor around Austin and along the Colorado River, while agriculture and grassland become more prominent toward the flatter eastern portions of the county.

2.1.3 Climate Classification

Austin is currently in International Code Council (ICC) / American Society of Heating, Refrigeration, and Air Conditioning Engineers (ASHRAE) Climate Zone 2A (hot–humid) and the Köppen–Geiger Cfa climate zone (humid subtropical), characterized by hot, humid summers and generally mild winters. Based on available projections under a 3.0 °C global warming scenario, Austin is not expected to shift into a different climate regime by 2050 or 2080, even as temperatures continue to increase within this classification.

Table 1

Year	ICC/ ASHRAE	Köppen–Geiger
2025	2A	Cfa (Humid Subtropical)
2050	2A	Cfa (Humid Subtropical)
2080	2A	Cfa (Humid Subtropical)

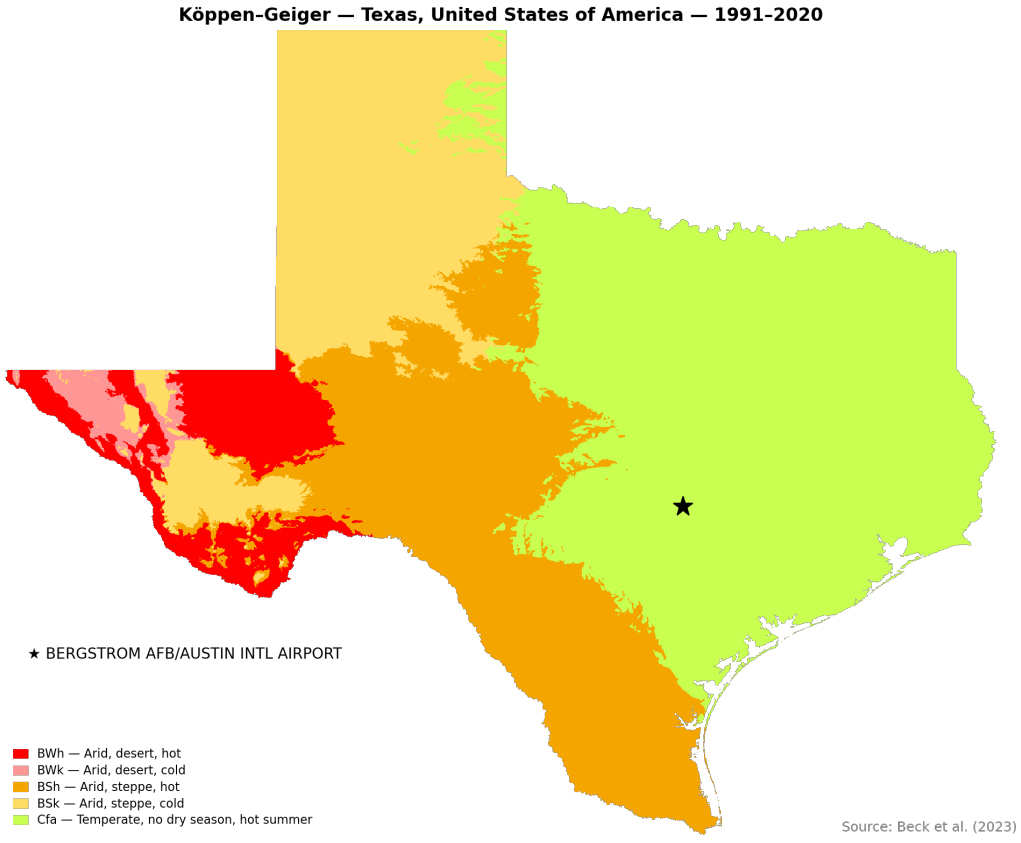

Figure 4 Köppen–Geiger climate zones across Texas for the 1991–2020 climatological period, with the location of Austin–Bergstrom International Airport indicated.

2.2 Monthly Average Conditions

Monthly climate projections show warming trends across all months with modest changes to precipitation and wind speeds. Summer maximum temperatures rise from current values of 94-98°F to 100-101°F by 2080, while winter minimum temperatures increase by 5-7°F over the same period. Annual precipitation decreases slightly from 33 inches currently to 31-32 inches in future periods, with late spring and early fall remaining the wettest months and late summer the driest. Wind speeds maintain their current seasonal pattern with minimal change.

2.2.1 Dry-Bulb Temperature

Current average daily maximum temperatures range from 64-68°F in winter (December-February) to 94-98°F in summer (June-August). March through May warm from 75°F to 87°F, while September through November cool from 92°F to 73°F. Average daily minimum temperatures span from 40-44°F in winter to 72-74°F in summer.

By 2050, maximum temperatures increase 2-3°F in most months. June reaches 95°F while July and August approach 99-100°F. Minimum temperatures increase 3-5°F, with winter lows rising to 44-47°F and summer lows to 74-76°F. By 2080, summer maximum temperatures reach 100-101°F (June, July, August) while winter maximums rise to 68-72°F. Minimum temperatures show larger increases, with winter lows rising to 46-50°F and summer lows reaching 76-78°F.

Uncertainty ranges span 3-7°F for maximum temperatures and 2-5°F for minimum temperatures, with wider ranges in winter and spring months. The ranges encompass model spread and natural climate variability.

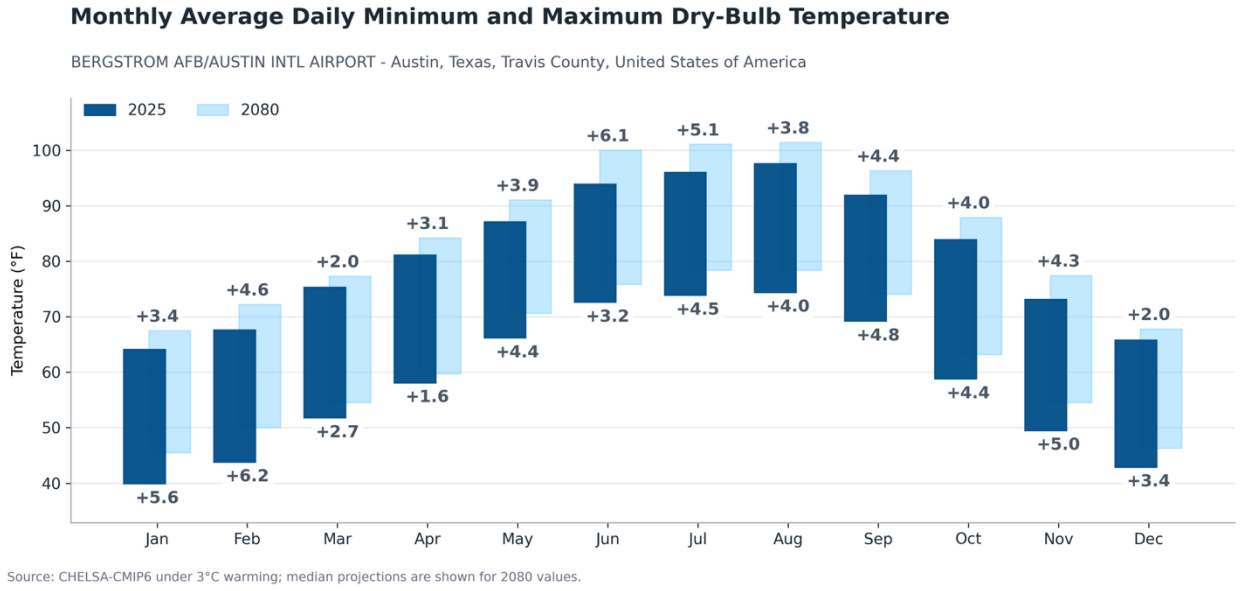

Figure 5 Monthly average daily minimum and maximum dry-bulb temperature for Austin–Bergstrom International Airport, comparing baseline conditions (2025) with late-century projections (2080). Values represent median projections under a global mean temperature pathway that reaches 3 °C of global warming by 2100.

2.2.2 Precipitation

Current annual precipitation totals 33.0 inches. Late spring and early fall receive the highest monthly amounts at 3.8-4.2 inches (May, June, October). Late summer is driest, with July at 2.1 inches and August at 1.8 inches. Winter and early spring months receive 2.1-2.6 inches per month.

Future projections show annual totals of 31-32 inches, a decrease of 1-2 inches from current conditions. Summer months become slightly drier (July and August dropping to 1.6-1.8 inches), while the wettest months decrease by 0.3-0.9 inches. Winter precipitation remains stable at 2.2-2.4 inches per month.

Monthly uncertainty ranges span 0.4-1.5 inches, with spring and fall months showing the widest ranges. Annual uncertainty spans approximately 4-6 inches around the central projection.

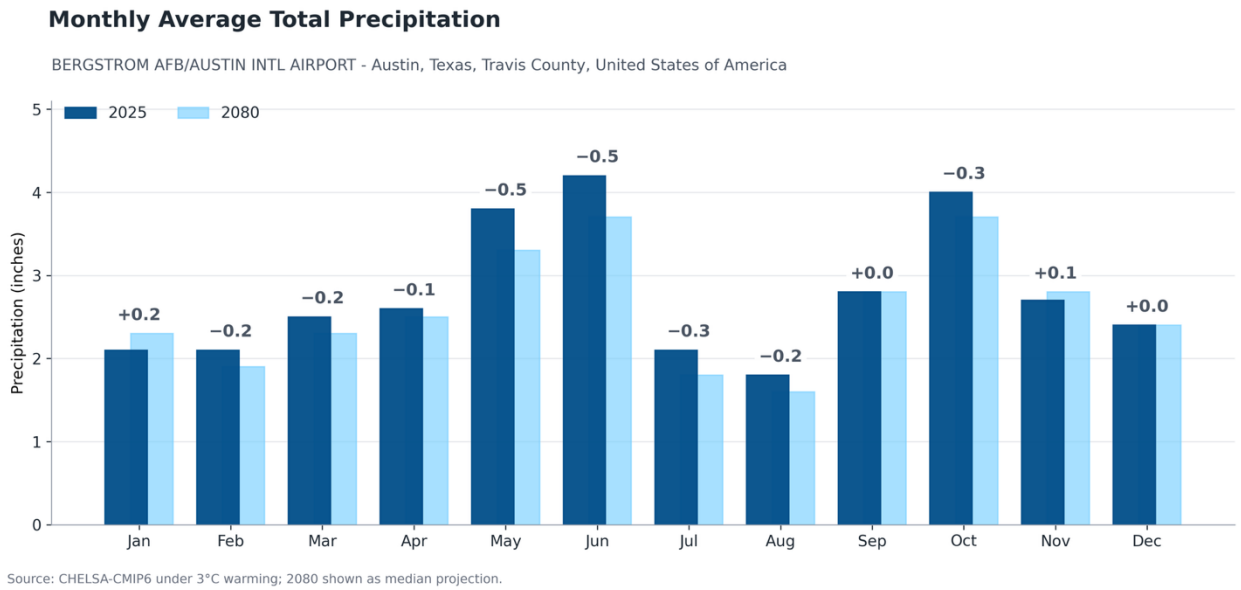

Figure 6 Monthly average total precipitation at Austin–Bergstrom International Airport, comparing baseline conditions (2025) with late-century projections (2080). Values represent median projections under a global mean temperature pathway that reaches 3 °C of global warming by 2100.

2.2.3 Wind Speed

Current wind speeds peak in late winter through spring (February-May at 9.0-9.4 mph) and reach their minimum in September (6.5 mph). Summer months range from 7.3 to 8.4 mph, while fall and winter months range from 7.1 to 9.2 mph.

Future projections show minimal change, with most months varying less than 0.5 mph from current conditions. The seasonal cycle persists, with spring maintaining the highest speeds (9.5-9.8 mph) and September the lowest (6.4-6.8 mph). Uncertainty ranges span 0.5-1.3 mph across months, comparable to or exceeding the projected changes in most cases.

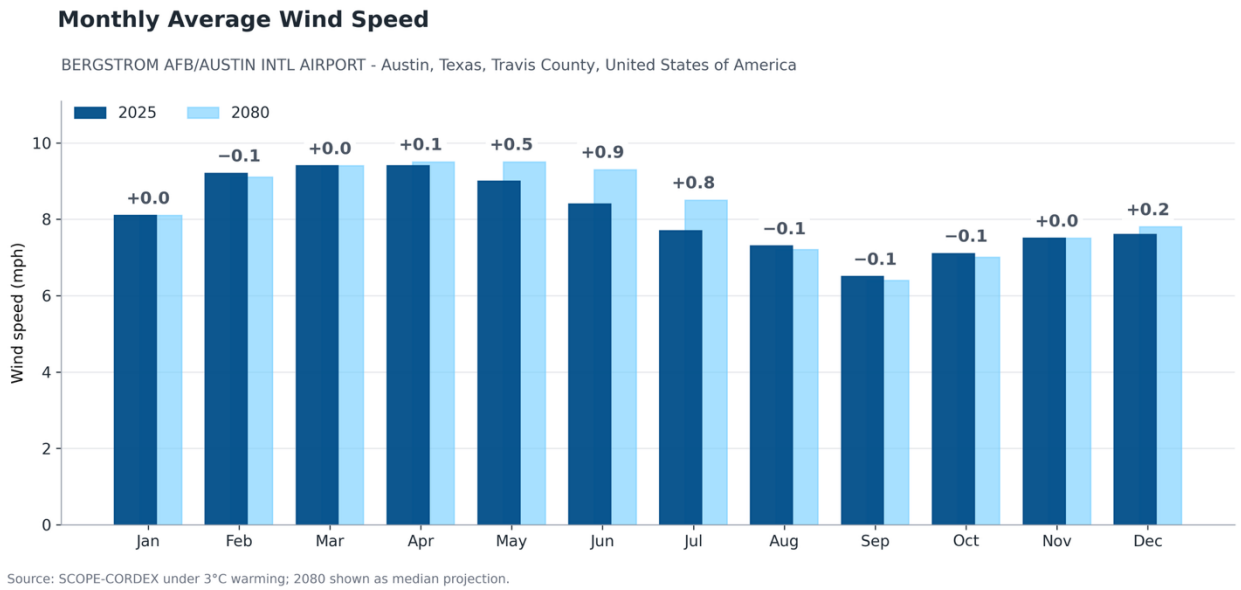

Figure 7 Monthly average wind speed at Austin–Bergstrom International Airport, comparing baseline conditions (2025) with late-century projections (2080). Values represent median projections under a global mean temperature pathway that reaches 3 °C of global warming by 2100.

3 Thermal and Psychrometric Loads

Temperature and humidity extremes determine HVAC capacity requirements, energy consumption, and thermal comfort in buildings. This section provides design dry-bulb and wet-bulb temperatures, humidity conditions, and degree days for current and future climates.

3.1 Heating Design

Heating design temperatures define the coldest conditions HVAC systems must handle to maintain interior comfort. Observed records from 1970-2024 show modest changes to heating-related indicators, while future projections indicate more substantial warming of extreme cold events. Given this discrepancy, conservative near-term design practice should consider favoring observed historical cold extremes over model projections that suggest warming of extremes that are inconsistent with observed trends.

3.1.1 Observed Heating-Related Trends

Historical observations show warming winters in Travis County, Texas. Heating degree days have declined significantly: -10.4% per decade (50°F base) and -5.8% per decade (65°F base) since 1979. Cold wave duration has decreased 10.2% per decade, while cold wave frequency shows a declining trend of 5.2% per decade (though this trend is not statistically significant). The annual number of days with minimum temperatures falling below freezing has also declined 6.6% per decade.

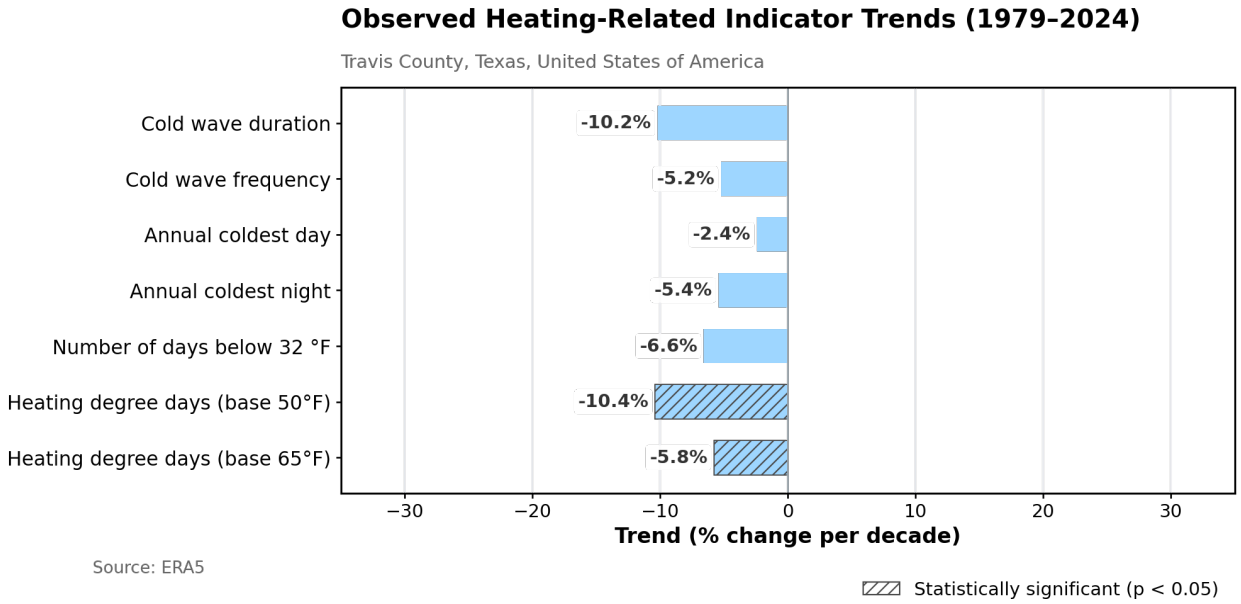

Figure 8 Observed trends in heating-related climate indicators for Travis County, Texas, over the period 1979–2024. Bars show percent change per decade based on ERA5 reanalysis data; hatched bars indicate trends that are statistically significant at the 5% level ($p < 0.05$).

3.1.2 Annual Heating Design Criteria

Annual Heating DB

Heating design temperatures increase under future warming. The 99% heating design temperature (coldest condition exceeded 99% of hours annually) rises from 30°F currently to 33°F by 2050 (range: 32-35°F) and 35°F by 2080 (range: 32-38°F). The more conservative 99.6% design temperature increases from 26°F currently to 30°F by 2050 (range: 28-32°F) and 32°F by 2080 (range: 28-35°F).

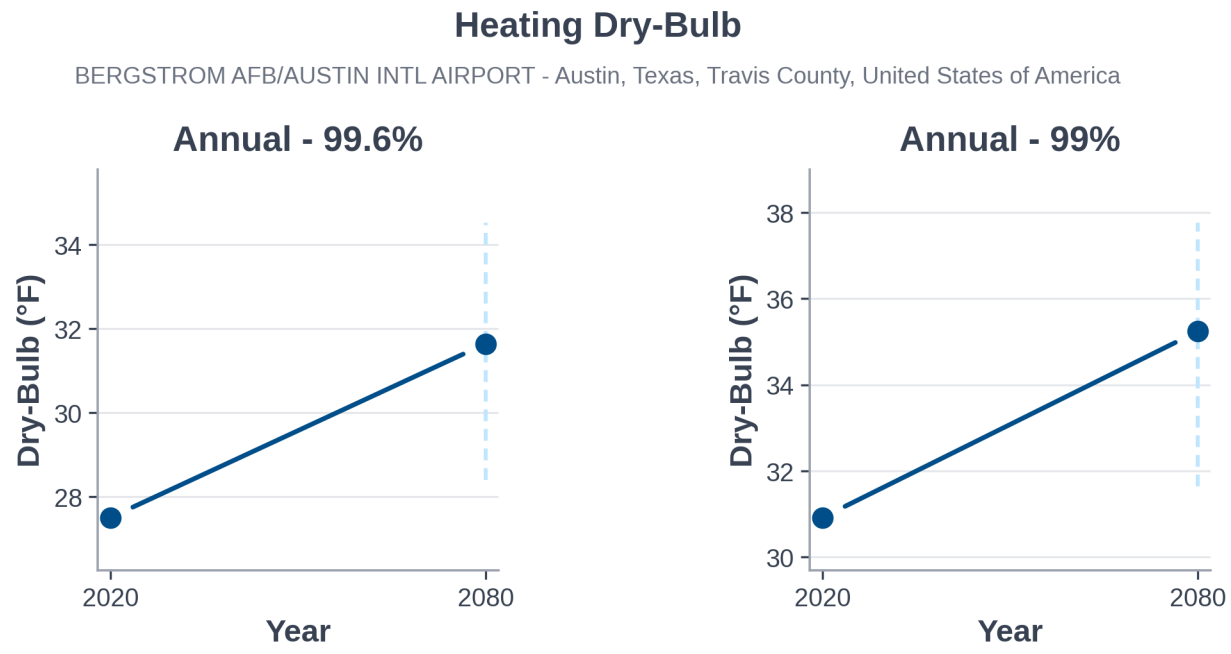

Figure 9 Projected changes in annual extreme heating dry-bulb temperature at Austin–Bergstrom International Airport, shown for the 99.6th and 99th percentiles. Values compare baseline conditions (2020) with late-century projections (2080) derived from projections under a pathway that reaches 3 °C of global warming by 2100. Dashed lines indicate the range of 90% of the models.

Table 2 Annual 99th and 99.6th percentile heating dry-bulb temperatures at Austin–Bergstrom International Airport for baseline (2020) and projected future periods (2050 and 2080) under a 3 °C global warming pathway.

°F	2020	2050	2080
99.6%	26.4	29.8 (28.4–31.8)	31.6 (28.4–34.5)
99%	29.7	33.3 (31.6–35.1)	35.2 (31.6–37.8)

3.1.3 Extreme Annual Minimum Dry-Bulb Temperatures

Extreme cold temperatures show substantial warming across all return periods. The coldest temperature in a typical year (2-year return period) warms from 19°F currently to 21-22°F by 2050 and 24°F by 2080. The 10-year cold extreme warms from 14°F to 17-18°F by mid-century and 18°F by 2080. For the 100-year cold extreme, temperatures rise from -1°F currently to 4°F by 2050 and 9°F by 2080, representing a 10°F increase in the century-scale cold extreme.

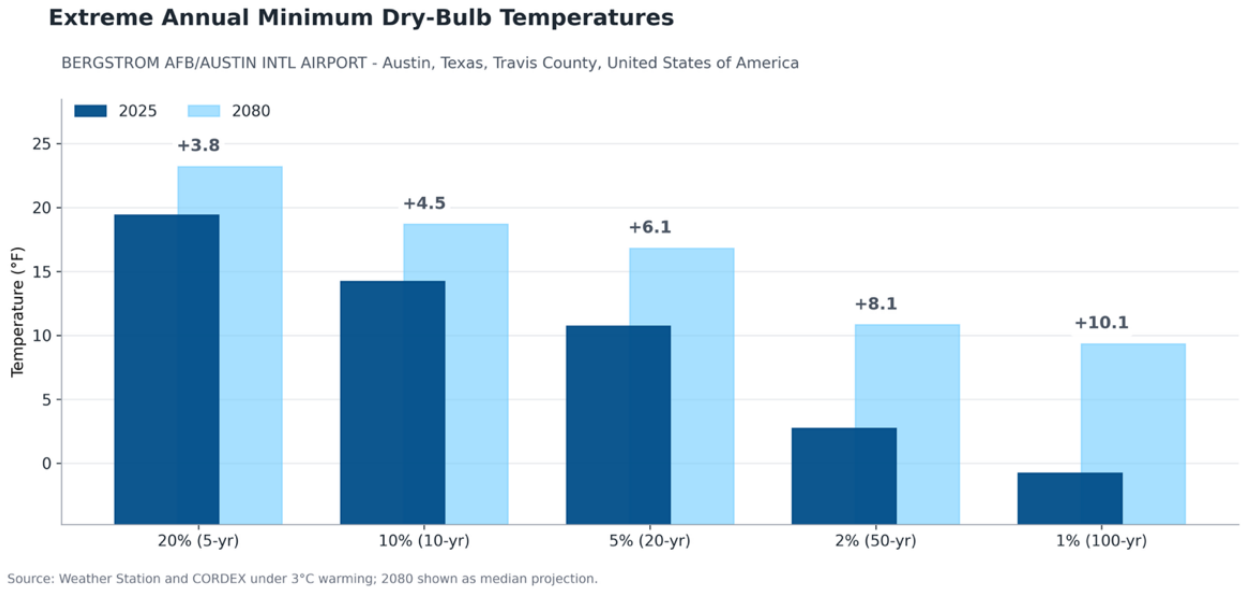

Figure 10 Extreme annual minimum dry-bulb temperatures at Austin–Bergstrom International Airport for selected exceedance probabilities (5-, 10-, 20-, 50-, and 100-year return periods), comparing baseline conditions (2025) with late-century projections (2080). Values represent median projections derived from weather-station observations and CORDEX simulations corresponding to approximately 3 °C of global mean warming.

Table 3 Annual extreme minimum dry-bulb temperature thresholds at Austin–Bergstrom International Airport across selected return periods, comparing baseline (2025) conditions with projected values for 2050 and 2080 under approximately 3 °C of global mean warming. Parenthetical ranges indicate inter-model variability.

°F	2025	2050	2080
20% (5-year)	19.4 (17.8–21.0)	21.9 (18.3–27.1)	23.2 (19.6–31.3)
10% (10-year)	14.2 (12.1–16.1)	17.1 (11.9–22.6)	18.7 (13.9–27.6)
5% (20-year)	10.7 (8.0–13.0)	13.9 (7.1–19.8)	16.8 (10.0–25.4)
2% (50-year)	2.7 (-1.7–6.4)	6.3 (-3.7–13.8)	10.8 (0.5–20.3)
1% (100-year)	-0.8 (-6.4–3.7)	3.5 (-9.1–11.3)	9.3 (-3.9–18.5)

3.1.4 Heating Degree Days

Annual heating degree days are projected to continue to decrease substantially under future warming. Using a 65°F base, current conditions show 1,619 HDD65, dropping to 1,320 by 2050 and 1,162 by 2080 (28% reduction). At a 50°F base, reductions are more pronounced: from 305 HDD50 currently to 143 by 2080 (53% reduction).

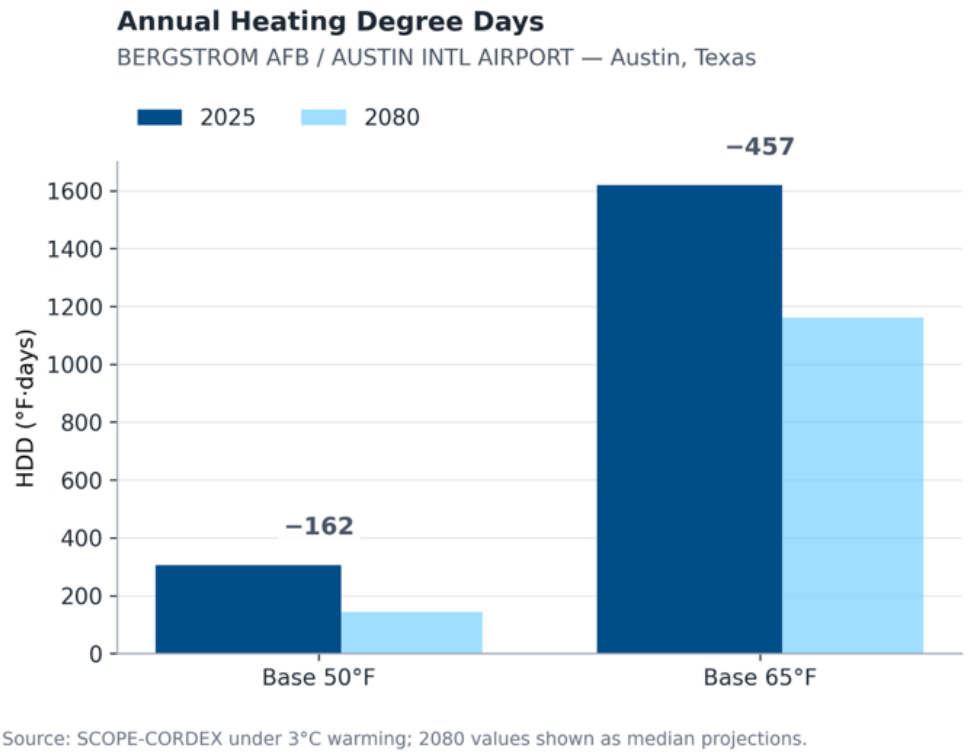

Figure 11 Annual heating degree days (HDD) at Austin–Bergstrom International Airport calculated using 50 °F and 65 °F base temperatures, comparing baseline conditions (2025) with late-century projections (2080). Values represent median SCOPE-CORDEX projections corresponding to approximately 3 °C of global mean warming.

Table 4 Annual heating degree days (HDD50 and HDD65) at Austin–Bergstrom International Airport for baseline (2025) and projected future periods (2050 and 2080) under approximately 3 °C of global mean warming.

Units: °F · Days	2025	2050	2080
HDD50	305	187 (140–231)	143 (76–211)
HDD65	1,619	1,320 (1,177–1,483)	1,162 (840–1,370)

3.2 Cooling Design

3.2.1 Observed Cooling-Related Trends

Historical observations show substantial increases in cooling-related indicators across Travis County, Texas. Heat wave duration has increased 23.9% per decade, the most dramatic change among all observed climate indicators. Heat wave frequency has increased 14.0% per decade, while very hot days (≥95°F) have increased 17.6% per decade. Hot days (≥86°F) and warm days (≥77°F) have increased 4.9% and 3.1% per decade respectively. Warm nights (above 68°F), cooling degree days (65°F base), and cooling degree days (50°F base) have all increased 4.0%, 5.3%, and 3.1% per decade respectively. The annual peak temperature shows the smallest change at 1.6% per decade. All metrics except annual peak temperature are statistically significant.

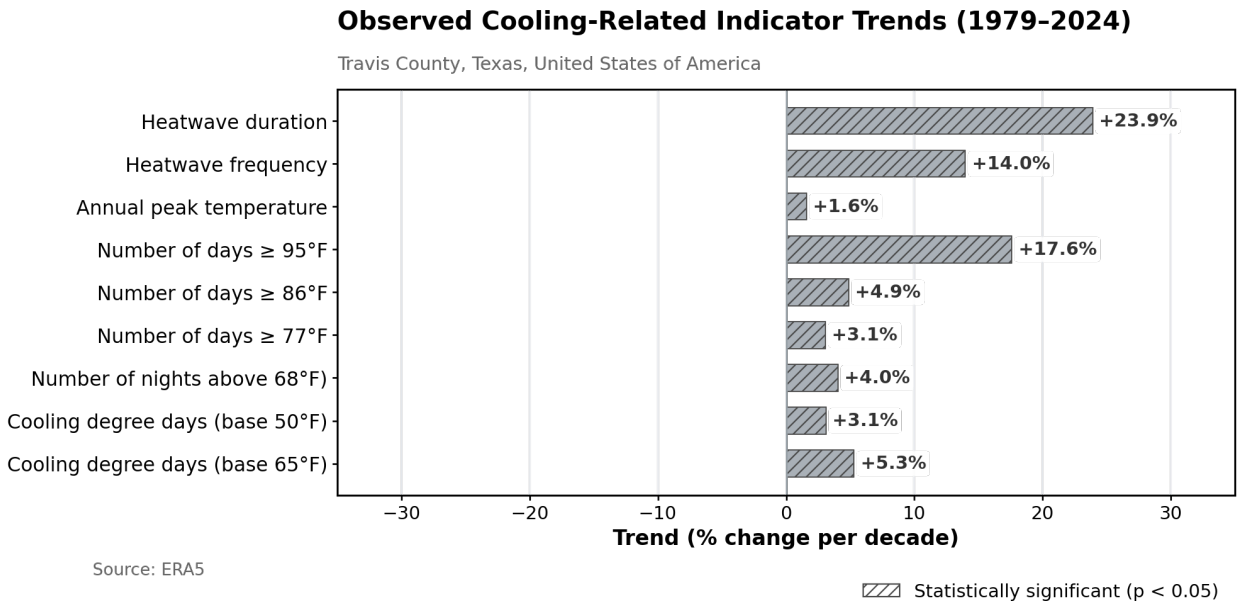

Figure 12 Observed trends in cooling-related climate indicators for Travis County, Texas, over the period 1979–2024. Bars show percent change per decade based on ERA5 reanalysis data; hatched bars indicate trends that are statistically significant at the 5% level (p < 0.05).

3.2.2 Annual Cooling Design Criteria

Annual Cooling DB/MCWB

Cooling design conditions increase across all frequency levels under future warming. The 0.4% condition (approximately 35 hours per year) shows dry-bulb temperatures rising from 98°F currently to 99°F by 2050 (range: 98-100°F) and 101°F by 2080 (range: 99-102°F), with mean coincident wet-bulb temperatures increasing from 74°F to 75°F by 2050 and 76°F by 2080. The 1% condition (88 hours per year) increases from 97°F to 98°F by 2050 and 100°F by 2080, while the 2% condition (175 hours per year) rises from 96°F to 97°F by 2050 and 99°F by 2080. Mean coincident wet-bulb temperatures show consistent increases of 1-2°F across all design frequencies, rising from current values of 74°F (0.4%), 74°F (1%), and 74°F (2%) to 76-77°F by 2080.

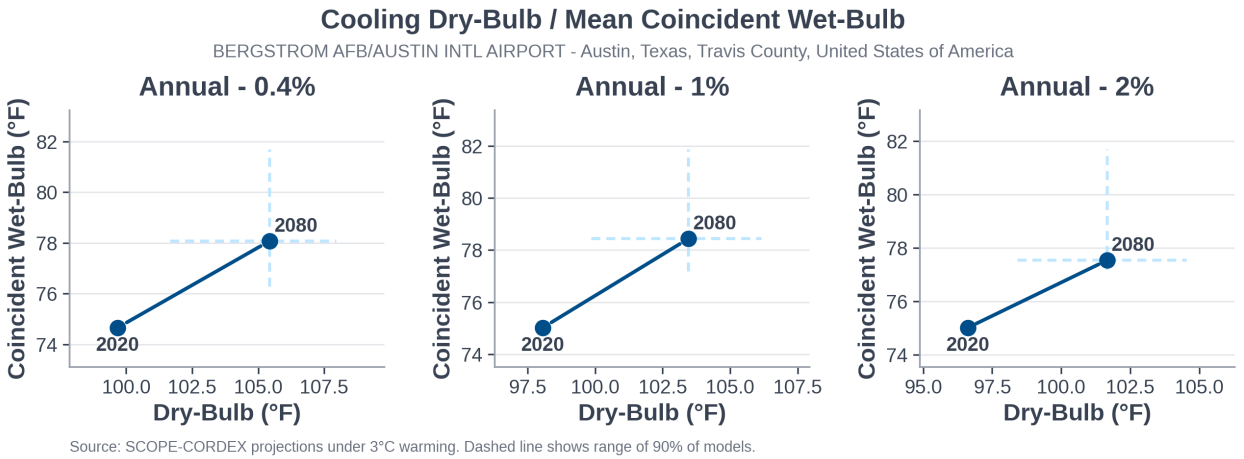

Figure 13 Projected annual cooling dry-bulb and coincident wet-bulb temperatures for selected exceedance probabilities at Austin–Bergstrom International Airport, comparing baseline (2020) and late-century (2080) conditions under ~3 °C global warming. Dashed lines show the 90% model range.

Table 5 Annual cooling dry-bulb and mean coincident wet-bulb temperatures at Austin–Bergstrom International Airport for selected exceedance probabilities, comparing baseline (2025) with mid- and late-century projections under ~3 °C global warming. Ranges denote the central 90% of model outcomes.

Units: °F	2020		2050		2080	
	DB	MCWB	DB	MCWB	DB	MCWB
2%	96.6	74.7	99.1 (97.5–100.8)	77.7 (75.9–79.0)	101.7 (98.4–104.5)	77.5 (77.2–81.7)
1%	98.1	75	100.6 (98.8–102.4)	77.4 (76.6–79.0)	103.5 (99.9–106.2)	78.4 (77.2–81.9)
0.4%	99.7	75	102.2 (100.4–104.0)	76.6 (75.9–78.6)	105.4 (101.7–108.0)	78.1 (76.3–81.7)

3.2.3 Extreme Annual Maximum Dry-Bulb Temperatures

Extreme heat intensifies across all return periods, with current rare events becoming substantially more frequent. The 100-year extreme increases from 115°F currently to 118°F by 2050 and 119°F by 2080. However, the frequency shift is more dramatic: today's 100-year heat event (115°F) becomes a 20-year event by 2080, while today's 50-year extreme (113°F) occurs approximately every 10 years. Current 20-year heat (110°F) becomes a typical 5-year event by 2080. For more common extremes, the typical annual maximum (5-year return period) increases from 107°F currently to 109°F by 2050 and 110°F by 2080. Uncertainty ranges span 3-6°F across return periods.

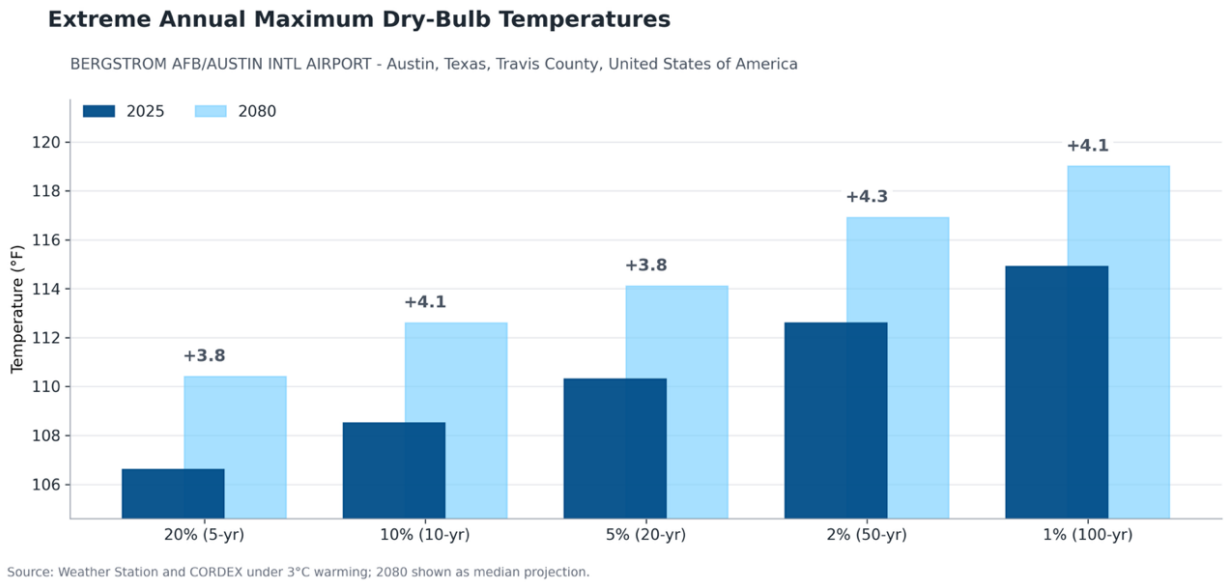

Figure 14 Extreme annual maximum dry-bulb temperatures at Austin–Bergstrom International Airport for selected exceedance probabilities (5-, 10-, 20-, 50-, and 100-year return periods), comparing baseline conditions (2025) with late-century projections (2080). Values represent median projections derived from weather station observations and models corresponding to approximately 3 °C of global mean warming.

Table 6 Projected extreme annual maximum dry-bulb temperatures (°F) at Austin–Bergstrom International Airport across multiple return periods for baseline, mid-century, and late-century conditions under 3 °C global warming.

Units: °F	2025	2050	2080
20% (5-year)	106.6 (105.9–108.3)	108.9 (108.2–110.6)	110.4 (109.7–112.1)
10%(10-year)	108.5 (107.0–110.2)	110.5 (109.0–112.2)	112.6 (111.1–114.3)
5% (20-year)	110.3 (108.9–112.5)	112.6 (111.2–114.8)	114.1 (112.7–116.3)
2%(50-year)	112.6 (111.0–114.8)	115.1 (113.5–117.3)	116.9 (115.3–119.1)
1% (100-year)	114.9 (111.9–117.9)	117.6 (114.6–120.6)	119.0 (116.0–122.0)

3.2.4 Cooling Degree Days

Annual cooling degree days increase substantially under future warming, indicating higher cooling energy demands. For the commonly used 65°F base, current conditions show 3,021 CDD65 annually, increasing to 3,561 by 2050 and 4,200 by 2080, representing increases of 18% and 39% respectively. Using a 50°F base, current conditions show 7,180 CDD50, rising to 7,885 by 2050 and 8,685 by 2080 (increases of 10% and 21%, respectively).

Observed trends show cooling degree days (65°F base) have increased 5.3% per decade from 1979-2024. Projections indicate CDD65 will continue increasing at approximately 7% per decade through 2080, about 35% faster than the historical rate.

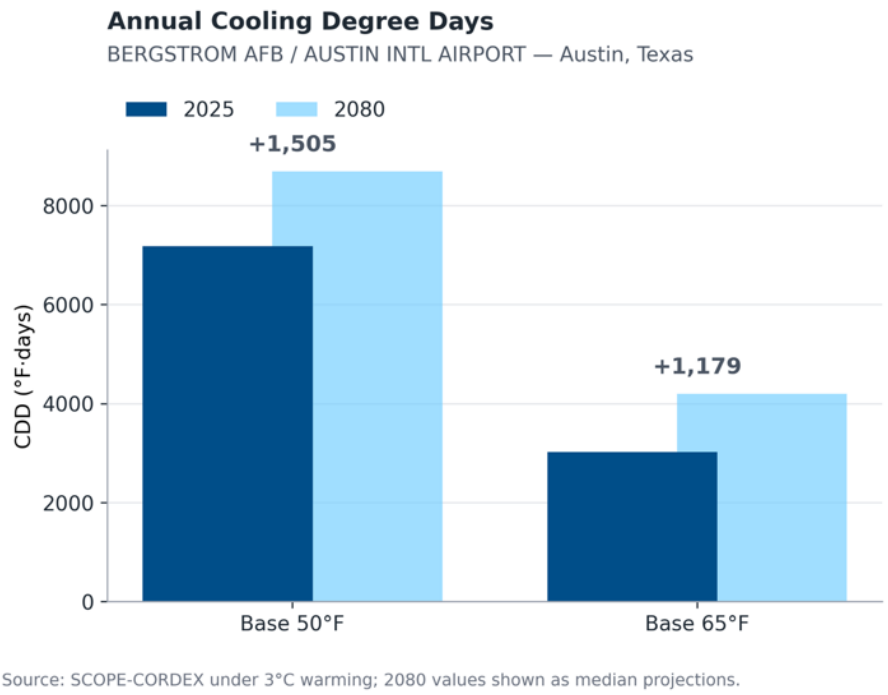

Figure 15 Projected changes in annual cooling degree days (CDD, °F·days) at Austin–Bergstrom International Airport for base temperatures of 50 °F and 65 °F, comparing baseline conditions (2025) with late-century projections (2080). Values represent median projections derived from SCOPE-CORDEX simulations corresponding to approximately 3 °C of global mean warming.

Table 7 Annual cooling degree days (CDD50 and CDD65) at Austin–Bergstrom International Airport for baseline (2025) and projected future periods (2050 and 2080) under approximately 3 °C of global mean warming.

Units: °F · Days	2025	2050	2080
CDD50	7,180	7,885 (7,428–8,104)	8,685 (7,719–9,166)
CDD65	3,021	3,561 (3,207–3,690)	4,200 (3,393–4,474)

3.2.5 Heatwave Projections

Daytime Heatwaves

Daytime heatwave frequency and duration increase substantially under future warming. Observed records show a gradual increase from approximately 1 event per year in the 1980s-1990s to 3-4 events per year in the 2020s. Future projections indicate acceleration of this trend, with heatwave frequency rising to approximately 5 events per year by 2050 and 6 events per year by 2080.

Heatwave duration follows a similar pattern, increasing from roughly 10 days per year in the 1980s to 25-30 days per year in the 2020s. By 2050, annual heatwave exposure reaches approximately 50 days, doubling to nearly 70 days per year by 2080. Uncertainty ranges widen substantially in future periods, with 2080 projections spanning from 40 to over 110 days per year, reflecting both model spread and natural climate variability in extreme heat occurrence.

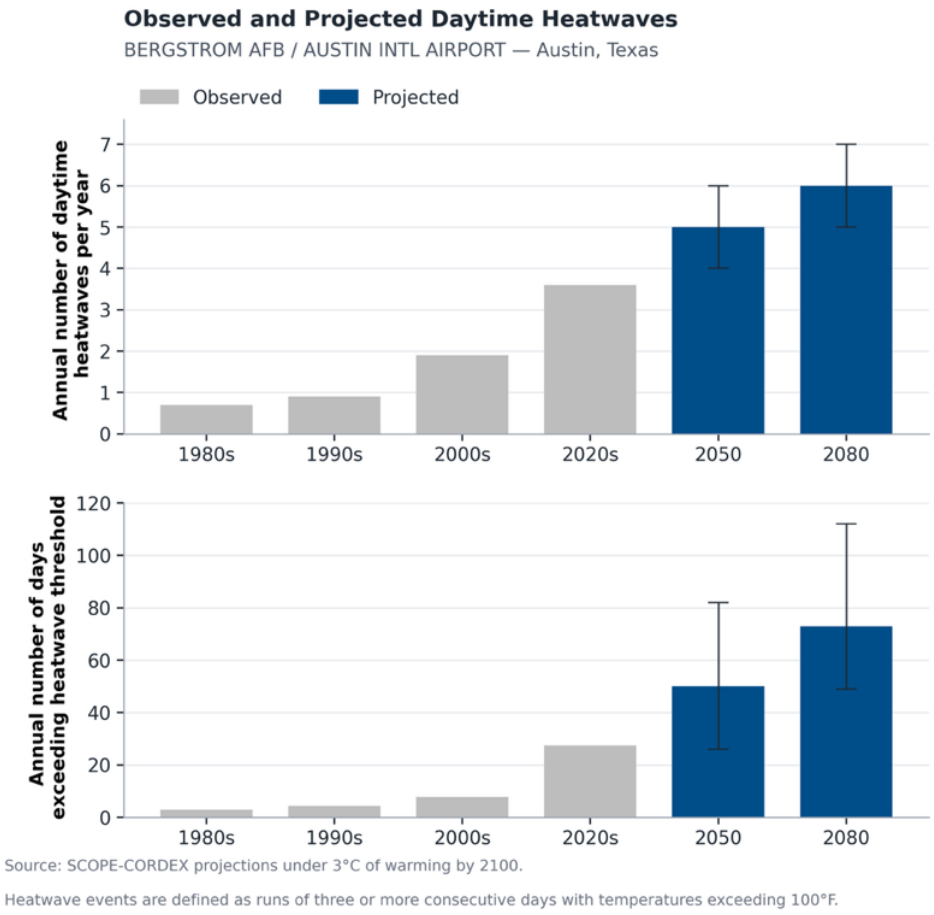

Figure 16 Observed and projected daytime heatwave events and exceedance days at Austin–Bergstrom International Airport, based on historical observations and SCOPE-CORDEX projections for ~3 °C global warming. Heatwaves are defined as ≥3 consecutive days with daily maximum temperature >100 °F; bars show median values and error bars indicate model spread.

Nighttime Heatwaves

Nighttime heatwave frequency and duration show dramatic increases under future warming. Observed records indicate a gradual rise from approximately 1 event per year in the 1980s-1990s to 4-5 events per year in the 2020s. Future projections show nighttime heatwave frequency nearly doubling to approximately 8 events per year by both 2050 and 2080.

Nighttime heatwave duration increases more substantially than frequency. Observed conditions show roughly 10 days per year in the 1980s rising to 20-25 days per year in the 2020s. By 2050, annual nighttime heatwave exposure reaches approximately 75 days, with further increases to over 100 days per year by 2080. Uncertainty ranges are wide, particularly for 2080 duration projections spanning from 60 to 120 days per year.

Nighttime heatwaves pose distinct risks compared to daytime events, as lack of overnight cooling limits heat stress recovery and increases strain on cooling systems operating continuously through 24-hour periods. The observed upward trend is already evident and aligns with projected acceleration.

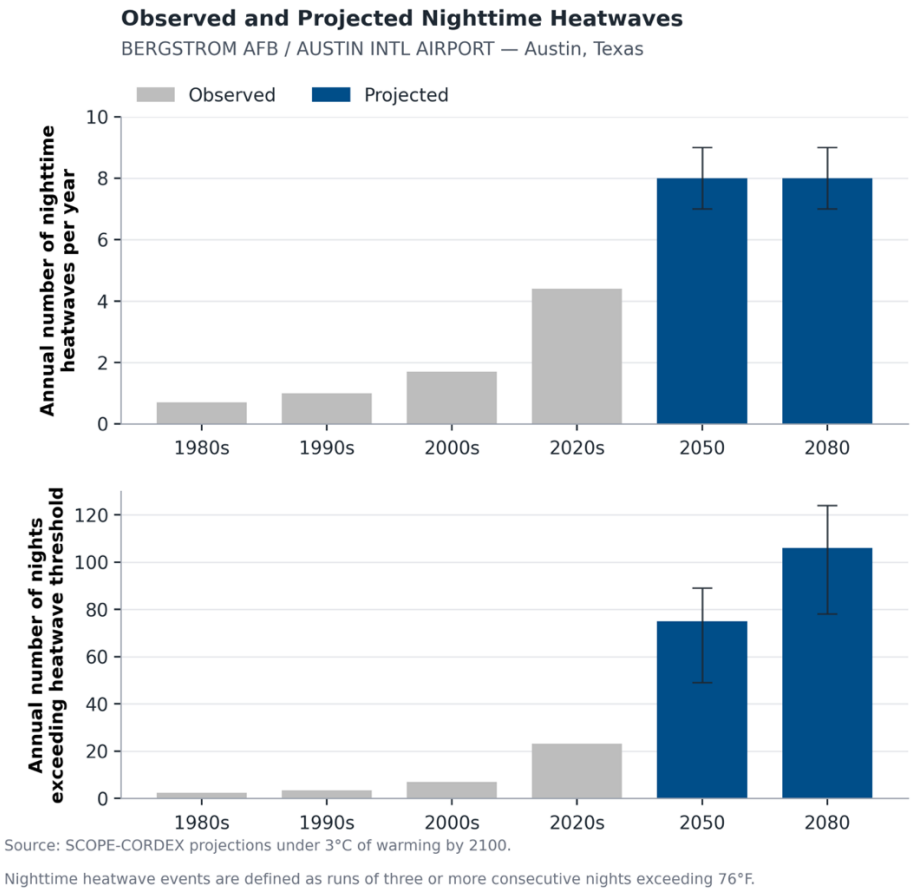

Figure 17 Observed and projected nighttime heatwave events and exceedance days at Austin–Bergstrom International Airport, based on historical observations and SCOPE-CORDEX projections for ~3 °C global warming. Heatwaves are defined as ≥3 consecutive days with daily minimum temperature >76 °F; bars show median values and error bars indicate spread of 90% of models.

3.3 Psychrometrics

Psychrometric design values define the combined temperature and humidity conditions used to size HVAC equipment and evaluate system performance. These include evaporation, dehumidification, and humidification design conditions based on mean coincident dry-bulb and wet-bulb temperatures or dew points.

3.3.1 Observed Humidity-Related Trends

Historical observations show modest increases in humidity-related indicators across Travis County, Texas. Average daily wet-bulb temperature has increased 1.2% per decade, while annual maximum wet-bulb temperature has increased 0.8% per decade—both statistically significant trends. Average humidity may be increasing. Daily average dew point has increased 1.2% per decade and annual maximum dew point has increased 0.5% per decade, though these trends are not statistically significant. The annual minimum dew point shows a declining trend of 3.1% per decade, suggesting dry extremes may be intensifying even as average humidity may be increasing.

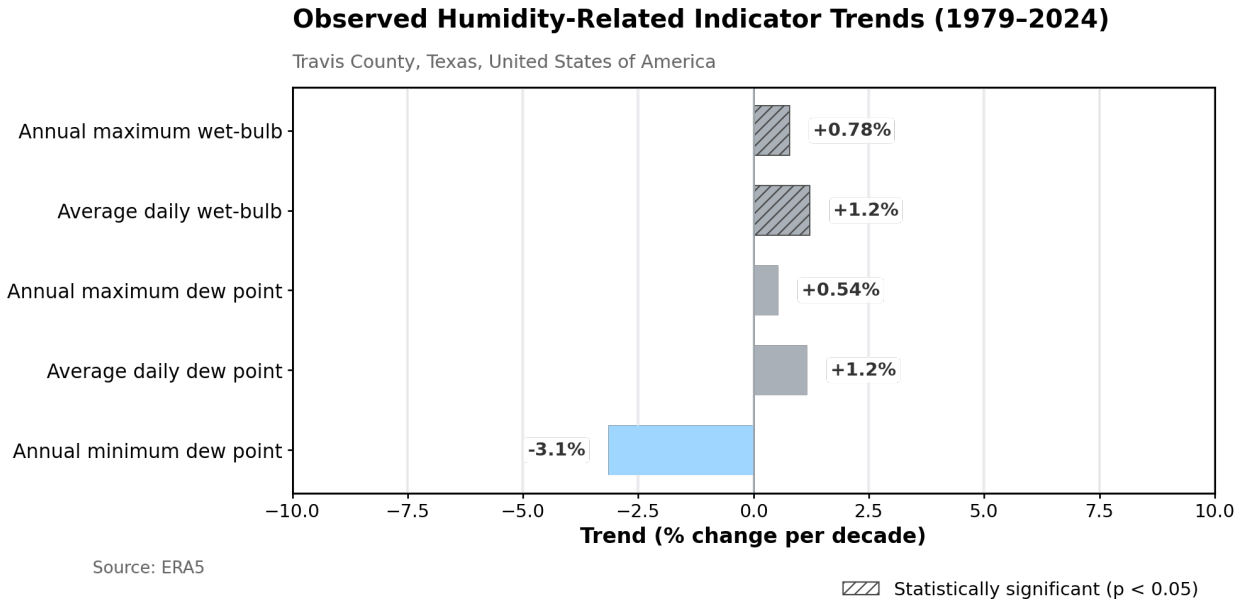

Figure 18 Long-term trends in humidity-related indicators for Travis County, Texas (1979–2024), expressed as percent change per decade. Small increases are observed in average and extreme wet-bulb and dew point temperatures, while minimum dew point shows a declining trend. Statistically significant trends ($p < 0.05$) are indicated by hatched bars.

3.3.2 Annual Humidity Design Criteria

Annual Evaporation WB/MCDB

Annual evaporation design wet-bulb temperatures increase across all frequency levels. The 0.4% condition (approximately 35 hours per year) rises from 79°F currently to 81°F by 2050 (range: 80-82°F) and 82°F by 2080 (range: 81-83°F), with mean coincident dry-bulb temperatures increasing from 93°F to 96-98°F. The 1% condition (88 hours per year) increases from 78°F to 80°F by 2050 and 81°F by 2080, while the 2% condition (175 hours per year) rises from 77°F to 79°F by 2050 and 80°F by 2080. These 2-3°F increases in design wet-bulb temperatures directly reduce cooling tower capacity and evaporative cooling effectiveness, requiring larger equipment or acceptance of reduced performance during peak conditions.

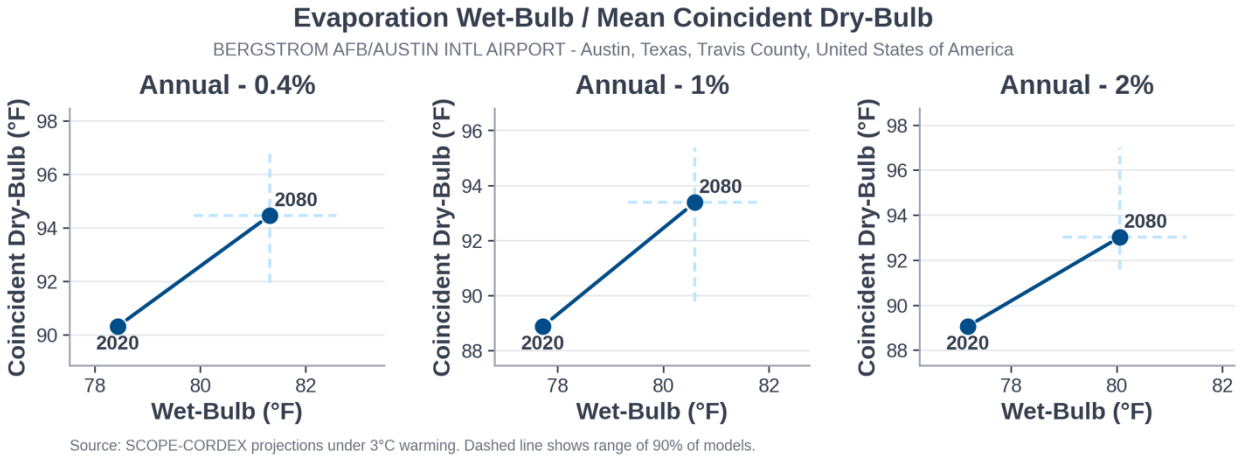

Figure 19 Projected changes in extreme evaporation-relevant conditions at Austin–Bergstrom International Airport, shown as coincident wet-bulb and dry-bulb temperature pairs for the 0.4%, 1%, and 2% annual exceedance levels. Points compare baseline conditions (2020) with late-century projections (2080) derived from SCOPE-CORDEX simulations corresponding to approximately 3 °C of global mean warming. Dashed lines indicate the central range encompassing 90% of models.

Table 8 Coincident wet-bulb and mean coincident dry-bulb temperature projections (°F) for Austin–Bergstrom International Airport at selected exceedance probabilities. Median values and central 90% model ranges are shown for 2050 and 2080 under ~3 °C global mean warming.

°F	2020		2050		2080	
	WB	MCDB	WB	MCDB	WB	MCDB
2%	77.2	89.1	79.0 (78.4–79.5)	91.6 (90.9–93.2)	80.1 (79.0–81.3)	93.0 (91.6–97.0)
1%	77.7	88.9	79.5 (79.0–80.1)	91.4 (90.0–93.0)	80.6 (79.3–81.9)	93.4 (89.8–95.4)
0.4%	78.4	90.3	80.1 (79.5–80.6)	92.8 (91.8–94.3)	81.3 (79.9–82.6)	94.5 (91.9–97.0)

Annual Dehumidification DP/MCDB

Annual dehumidification design dew points show similar warming patterns. The 0.4% condition increases from 76°F currently to 78°F by 2050 (range: 77-79°F) and 79°F by 2080 (range: 78-80°F), with mean coincident dry-bulb temperatures rising from 87°F to 90-91°F. The 1% and 2% conditions follow comparable trends, with 2-3°F increases across all metrics. Higher dew points indicate increased latent cooling loads and reduced dehumidification efficiency, particularly for systems relying on cooling coil condensation or desiccant dehumidification.

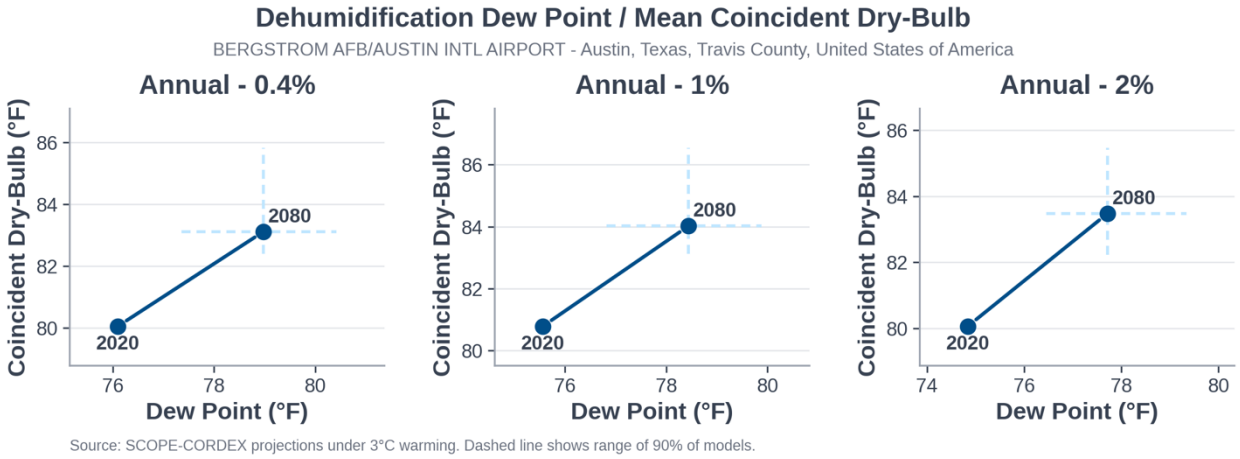

Figure 20 Projected changes in annual dehumidification design dew point (DP) and mean coincident dry-bulb temperature (MCDB) at Austin–Bergstrom International Airport for the 0.4%, 1%, and 2% exceedance probabilities. Points compare baseline conditions (2020) with late-century projections (2080) derived from SCOPE-CORDEX simulations corresponding to approximately 3 °C of global mean warming; dashed lines indicate the central 90% model range.

Table 9 Projected annual dehumidification DP and coincident dry-bulb temperature (°F) for baseline, mid-century, and late-century conditions under ~3 °C global mean warming.

°F	2020		2050		2080	
	DP	MCDB	DP	MCDB	DP	MCDB
2%	74.8	80.1	76.8 (75.9–77.4)	82.2 (81.9–83.7)	77.7 (76.5–79.3)	83.5 (82.2–85.5)
1%	75.6	80.8	77.4 (76.3–77.7)	83.1 (81.3–84.0)	78.4 (76.8–79.9)	84.0 (83.1–86.5)
0.4%	76.1	80.1	77.9 (76.8–78.3)	82.4 (80.6–83.3)	79.0 (77.4–80.4)	83.1 (82.4–85.8)

Annual Humidification DP/MCDB

Winter humidification requirements decrease as design dew points warm. The 99.6% condition (coldest/driest 53 hours per year) rises from 19°F currently to 22°F by 2050 (range: 20-24°F) and 24°F by 2080 (range: 22-26°F), with mean coincident dry-bulb temperatures increasing from 28°F to 31-33°F. The 99% condition shows similar warming of 3-4°F. These increases reduce humidification loads for buildings maintaining interior humidity levels during winter, lowering energy consumption and equipment capacity requirements for humidification systems.

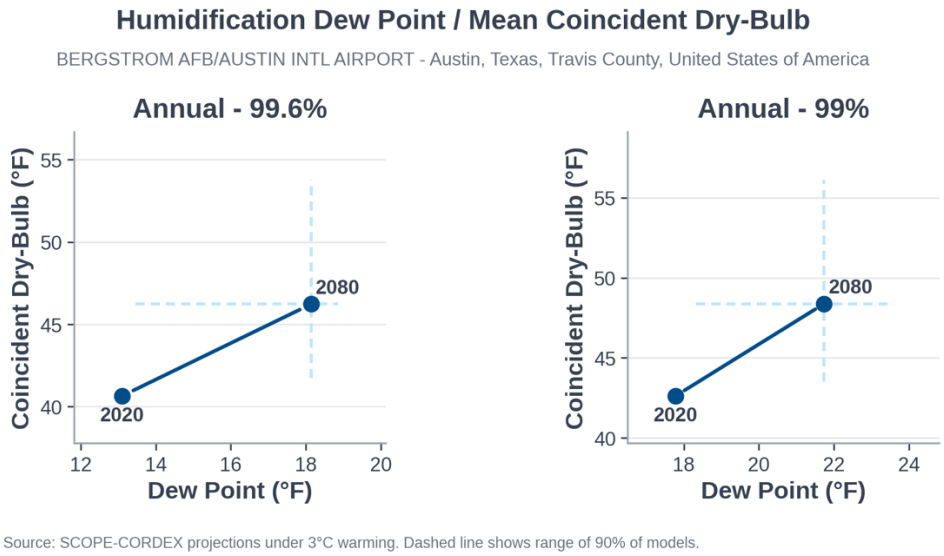

Figure 21 Projected changes in annual humidification design dew point (DP) and mean coincident dry-bulb temperature (MCDB) at Austin–Bergstrom International Airport for the 99.6% and 99% exceedance probabilities. Points compare baseline conditions (2020) with late-century projections (2080) derived from SCOPE-CORDEX simulations corresponding to approximately 3 °C of global mean warming; dashed lines indicate the central 90% model range.

Table 10 Projected annual humidification DP and coincident dry-bulb temperature (°F) under ~3 °C global mean warming.

°F	2020		2050		2080	
	DP	MCDB	DP	MCDB	DP	MCDB
99%	17.8	42.6	20.3 (18.5–22.3)	46.4 (42.8–50.7)	21.7 (18.3–23.5)	48.4 (43.5–56.1)
99.6%	13.1	40.6	16.5 (13.8–17.2)	44.8 (41.9–48.0)	18.1 (13.5–18.9)	46.2 (41.7–53.8)

4 Hydrology and Drainage

4.1 Observed Precipitation-Related Trends

Historical observations show mixed precipitation trends across Travis County, Texas, though none are statistically significant. Consecutive dry days have increased 7.1% per decade, while very heavy rain days (≥20 mm/day) have increased 3.0% per decade. Maximum 1-day and 5-day precipitation have increased 4.0% and 2.5% per decade respectively, and annual maximum hourly precipitation has increased 2.2% per decade. Annual total precipitation shows no trend, suggesting precipitation is becoming more variable with intensifying extremes.

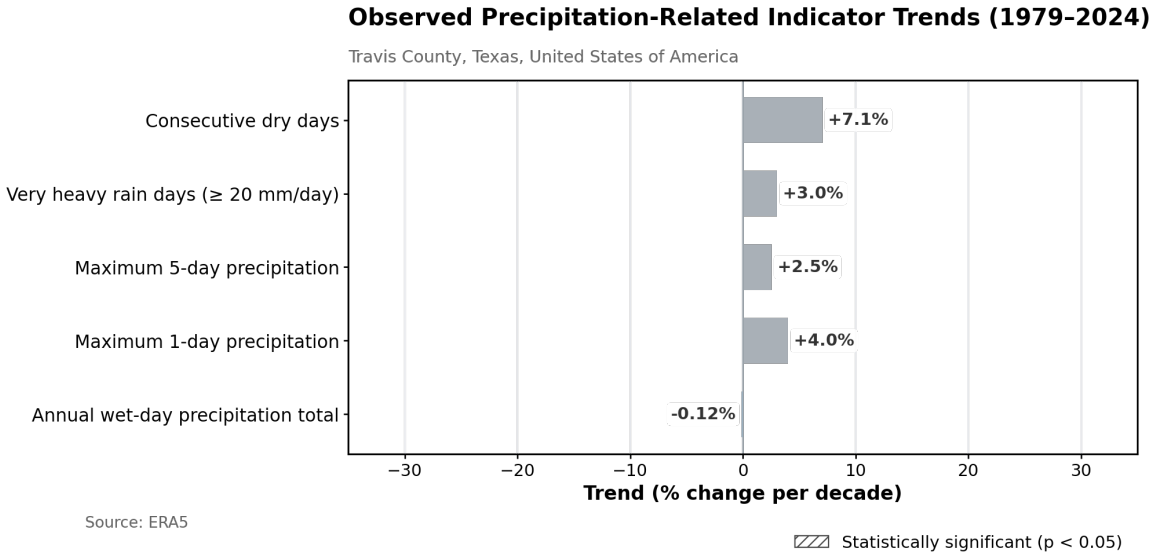

4.2 Precipitation Extremes

4.2.1 Event duration–1 hour

Extreme 1-hour rainfall totals increase across all return periods. The 5-year and 10-year events show modest increases of 0.1-0.2 inches through 2080, while rarer events intensify more substantially, with the 1,000-year rainfall increasing from 7.1 inches currently to 7.5 inches by 2080. These intensification trends mean that current 10-year conditions (3.0 inches) become approximately 7-year events by 2080 (median projection).

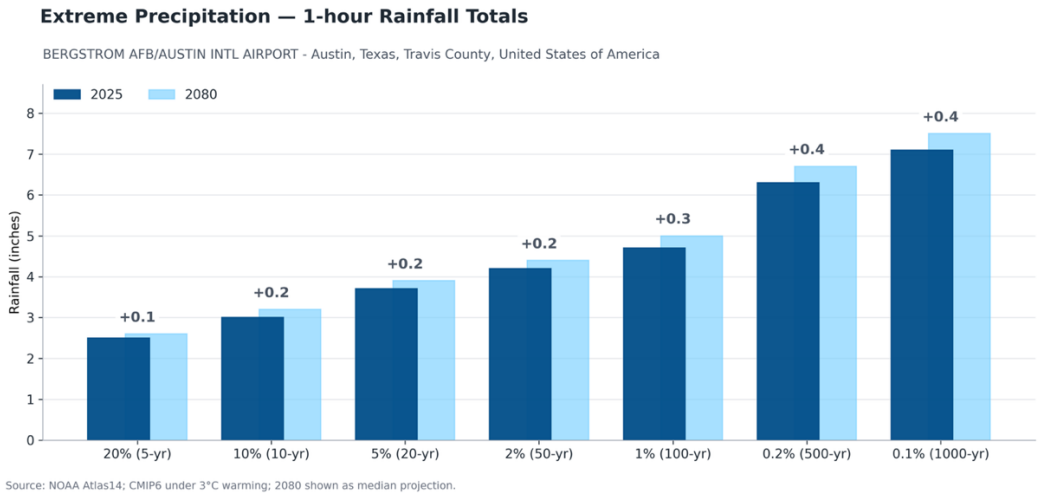

Figure 22 Projected 1-hour extreme rainfall depths at Austin–Bergstrom International Airport across selected return periods (5–1,000 years), comparing baseline conditions (2025) with late-century projections (2080). Values show median changes derived from NOAA Atlas 14 and CMIP6 simulations under approximately 3 °C of global mean warming.

Table 11 Projected 1-hour extreme rainfall depths (inches) at Austin–Bergstrom International Airport for selected return periods under baseline (2025), mid-century (2050), and late-century (2080) conditions.

inches	2025	2050	2080
20% (5-year)	2.5 (1.9–3.3)	2.6 (2.0–3.4)	2.6 (2.0–3.5)
10%(10-year)	3.0 (2.2–4.0)	3.1 (2.3–4.1)	3.2 (2.3–4.2)
5% (20-year)	3.7 (2.7–5.0)	3.8 (2.8–5.2)	3.9 (2.9–5.3)
2%(50-year)	4.2 (2.9–5.9)	4.3 (3.0–6.1)	4.4 (3.1–6.2)
1% (100-year)	4.7 (3.3–6.9)	4.9 (3.4–7.1)	5.0 (3.5–7.3)
0.2% (500-year)	6.3 (4.1–9.8)	6.5 (4.2–10.1)	6.7 (4.3–10.4)
0.1% (1000-year)	7.1 (4.5–11.3)	7.3 (4.7–11.7)	7.5 (4.8–11.9)

4.2.2 Event duration–24 hour

Extreme 24-hour rainfall totals increase across all return periods, with implications for prolonged flooding, reservoir management, and multi-day storm impacts. The 5-year and 10-year events show modest increases of 0.3-0.4 inches through 2080, while rarer events intensify more substantially, with the 1,000-year rainfall increasing from 22.0 inches currently to 23.2 inches by 2080. These intensification trends mean that current 10-year conditions (6.9 inches) become approximately 8-year events by 2080 (median projection).

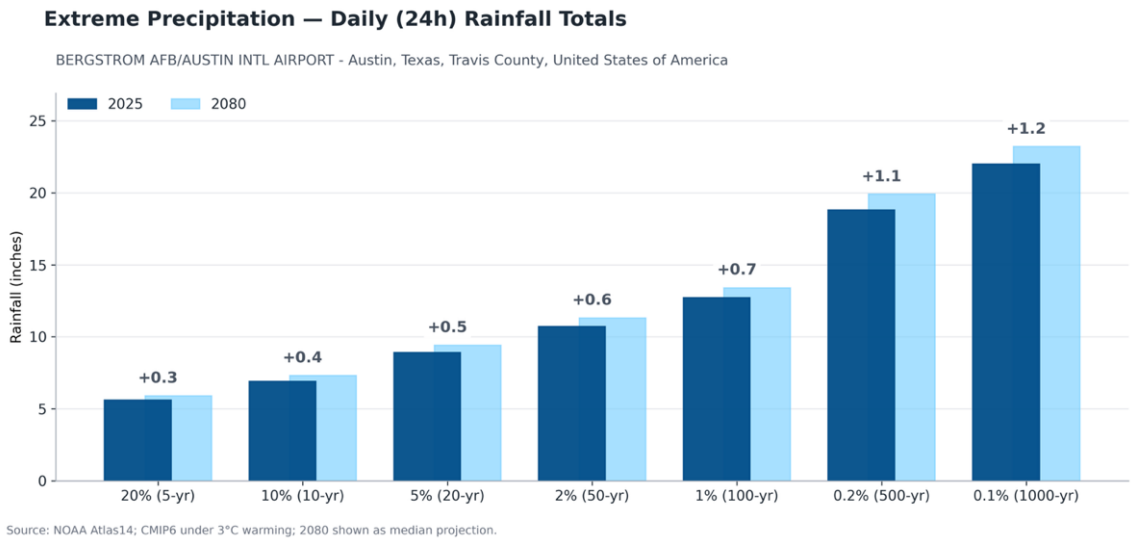

Figure 23 Projected 24-hour extreme rainfall totals at Austin–Bergstrom International Airport across selected return periods, comparing baseline (2025) and late-century (2080) conditions.

Table 12 Projected 24-hour extreme rainfall depths (inches) at Austin–Bergstrom International Airport for selected return periods under baseline (2025), mid-century (2050), and late-century (2080) conditions.

inches	2025	2050	2080
20% (5-year)	5.6 (4.4–7.0)	5.8 (4.6–7.2)	5.9 (4.6–7.4)
10%(10-year)	6.9 (5.4–8.8)	7.1 (5.6–9.1)	7.3 (5.7–9.3)
5% (20-year)	8.9 (6.7–11.8)	9.2 (6.9–12.2)	9.4 (7.1–12.5)
2%(50-year)	10.7 (7.8–14.5)	11.1 (8.1–15.0)	11.3 (8.2–15.3)
1% (100-year)	12.7 (9.0–17.6)	13.1 (9.3–18.2)	13.4 (9.5–18.6)
0.2% (500-year)	18.8 (12.5–27.6)	19.4 (12.9–28.5)	19.9 (13.2–29.2)
0.1% (1000-year)	22.0 (14.2–32.9)	22.8 (14.7–34.0)	23.2 (15.0–34.7)

5 Structural Loads and Geotechnical

5.1 Wind Loading

Extreme wind gusts show little change for more frequent events but substantial intensification in the tail of the distribution driven by changes in tropical cyclone behavior. While the 50-year and 100-year gusts increase by only 0-1 miles per hour (mph) through 2050, the rarest events show larger changes, with the 10,000-year gust increasing by 14 mph (from 127 to 141 mph).

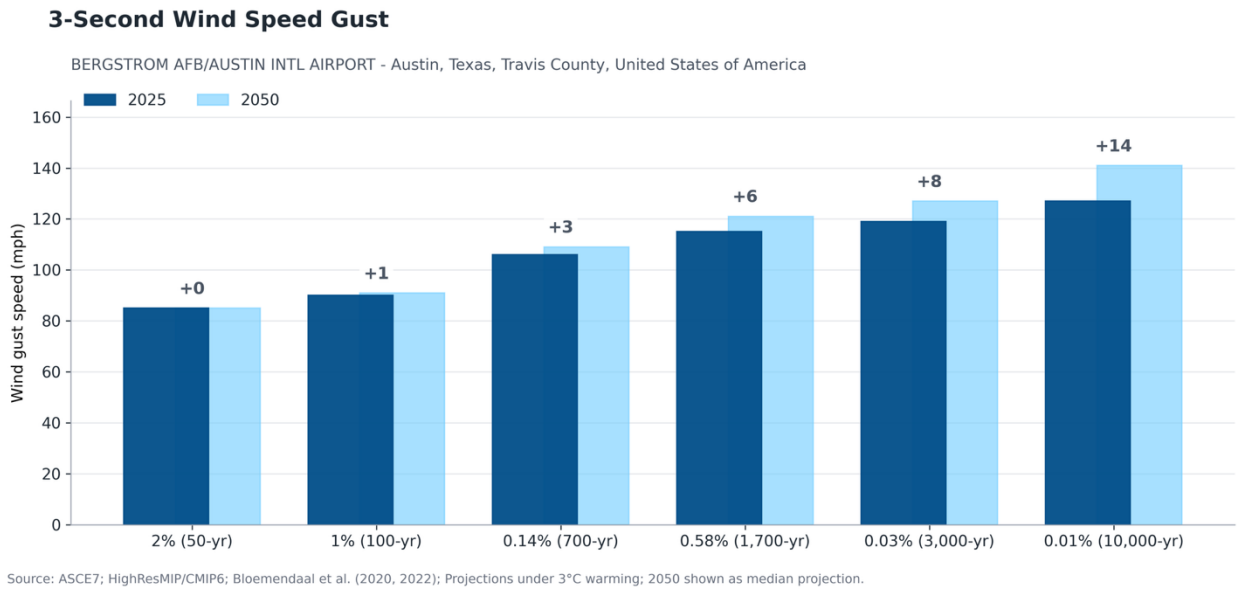

Figure 24 Projected 3-second peak wind gust speeds at Austin–Bergstrom International Airport across selected exceedance probabilities (50- to 10,000-year return periods), comparing baseline conditions (2025) with mid-century projections (2050). Projections reflect combined non-tropical cyclone winds and tropical cyclone wind fields under approximately 3 °C of global mean warming.

Table 13 Projected 3-second extreme wind gust speeds (mph) at Austin–Bergstrom International Airport for selected return periods under baseline (2025) and mid-century (2050) conditions. Values represent median projections, with ranges indicating the central model spread.

miles per hour	2025	2050
2% (50-year)	85	85 (79–92)
1% (100-year)	90	91 (89–94)
0.14% (700-year)	106	109 (106–112)
0.58% (1,700-year)	115	121 (115–128)
0.03% (3,000-year)	119	127 (120–132)
0.01% (10,000-year)	127	141 (123–144)

5.2 Geotechnical Stress

5.2.1 Current Drought Trends

Observed Texas drought extent since 1940 shows episodic occurrences of major widespread drought followed by recovery periods. Four major statewide drought episodes are evident: the 1950s, the mid-1960s drought, the severe 2011 event, and the recent 2021–2024 period, each affecting 70-100% of the state at their peaks. Overall, there is no clear increasing trend over the past eighty-five years.

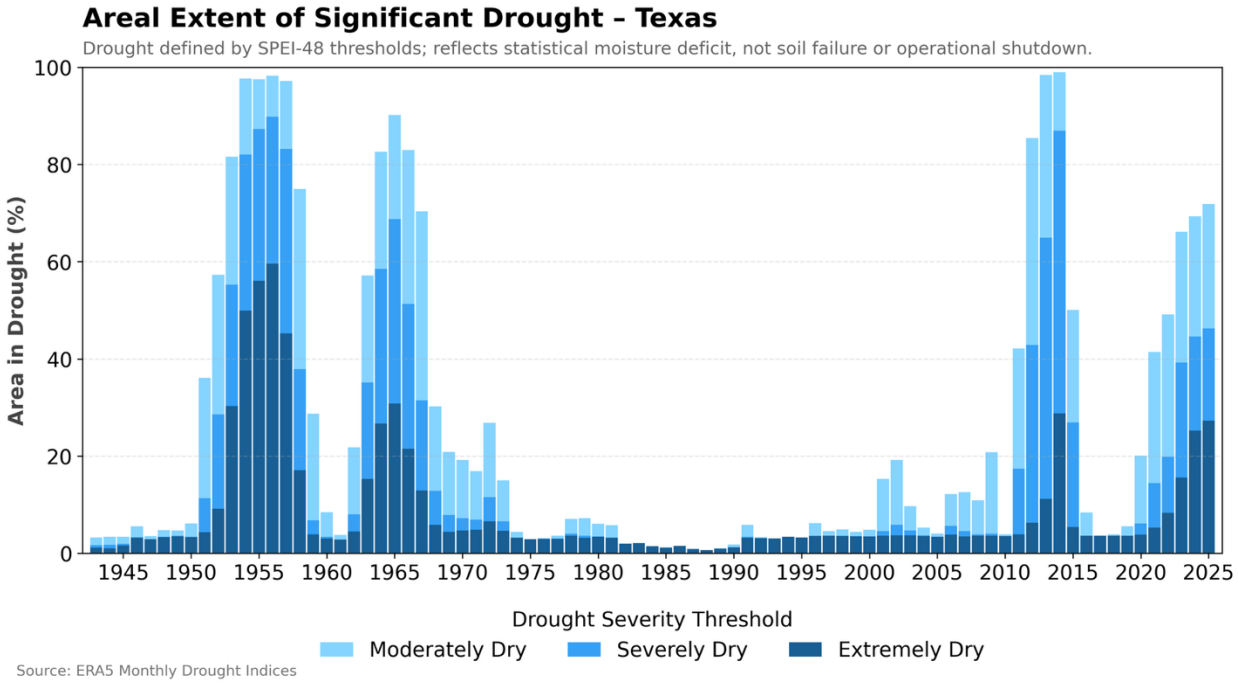

Figure 25 Historical areal extent of significant drought across Texas (1940s–2020s), showing the percentage of the state experiencing moderate, severe, and extreme drought based on SPEI-48 thresholds. Values reflect long-term statistical moisture deficits derived from ERA5 monthly drought indices, not direct measures of soil failure or operational impact.

About Standardized Precipitation–Evapotranspiration Index

SPEI-48 (Standardized Precipitation–Evapotranspiration Index, 48-month timescale) quantifies cumulative climatic water balance (precipitation minus evapotranspiration) over a rolling four-year period. By incorporating temperature-driven evaporative demand in addition to precipitation, SPEI-48 captures warming-induced drying and identifies persistent wet and dry regimes that influence groundwater levels, long-term soil moisture, and hydrologic recovery times.

SPEI-48 helps evaluate whether historical subsurface conditions used for design remain representative under a changing climate. Sustained negative SPEI-48 values indicate prolonged drying that can result in cumulative soil shrinkage, differential settlement, loss of matric suction, desiccation cracking, and changes in shear strength—providing critical context for assessing ground performance affecting foundations, pavements, slopes, and earth structures with long service lives.

6 Solar Photovoltaic Resources

6.1 Current Cloudiness Trends

From 1979–2024, monthly cloud cover trends in Austin show statistically significant increase in cloud cover in July and weaker, non-significant changes in most other months. Winter and early fall months tend toward decreasing cloud cover, indicating clearer conditions outside of summer.

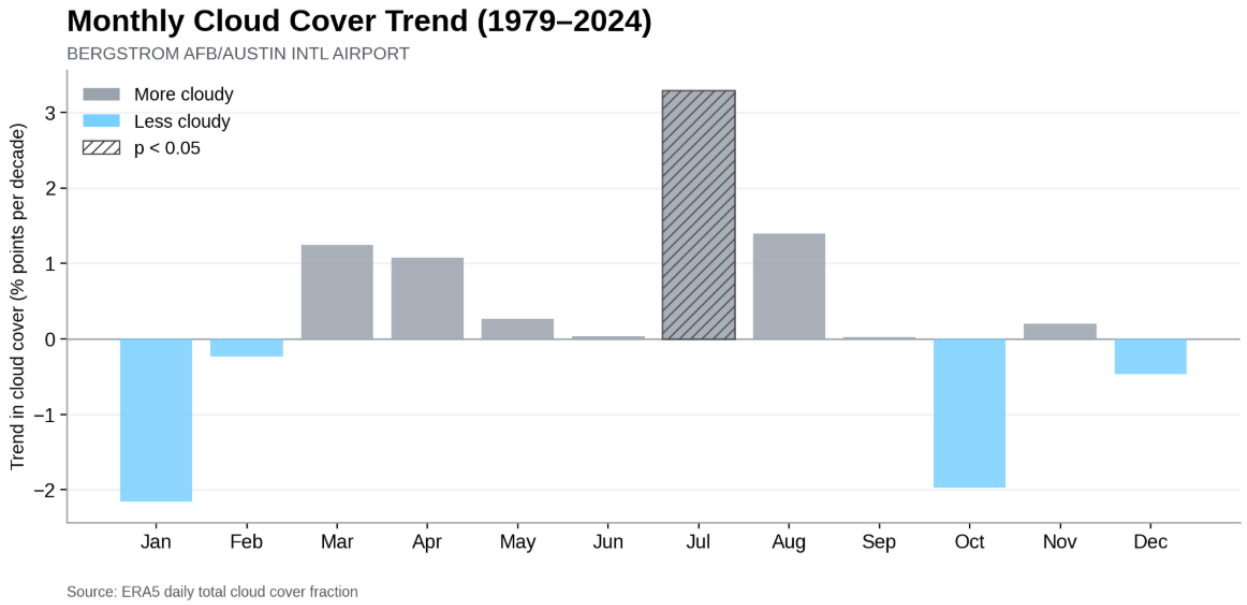

Figure 26 Observed monthly trends in total cloud cover at Austin–Bergstrom International Airport for 1979–2024, expressed as percentage-point change per decade. Positive values indicate increasing cloudiness and negative values indicate decreasing cloudiness; hatched bars denote statistically significant trends ($p < 0.05$) based on ERA5 daily cloud fraction data.

6.2 Current and Future Global Horizontal Irradiance (GHI)

Monthly average Global Horizontal Irradiance (GHI) in Austin increases consistently from present-day through mid- and late-century, with the largest gains in late spring and summer. By 2080, median monthly GHI rises by roughly 1–3 Btu/ft²/day, peaking in June–August, indicating a modest but systematic strengthening of the solar resource. Smaller but persistent winter increases suggest a year-round upward shift rather than a seasonal redistribution.

Projection uncertainty is moderate and seasonally variable, with the widest ranges in late spring and summer due to inter-model spread. While monthly projections span several Btu/ft²/day around the median, most models agree on higher future GHI, meaning uncertainty affects the magnitude of change more than its direction.

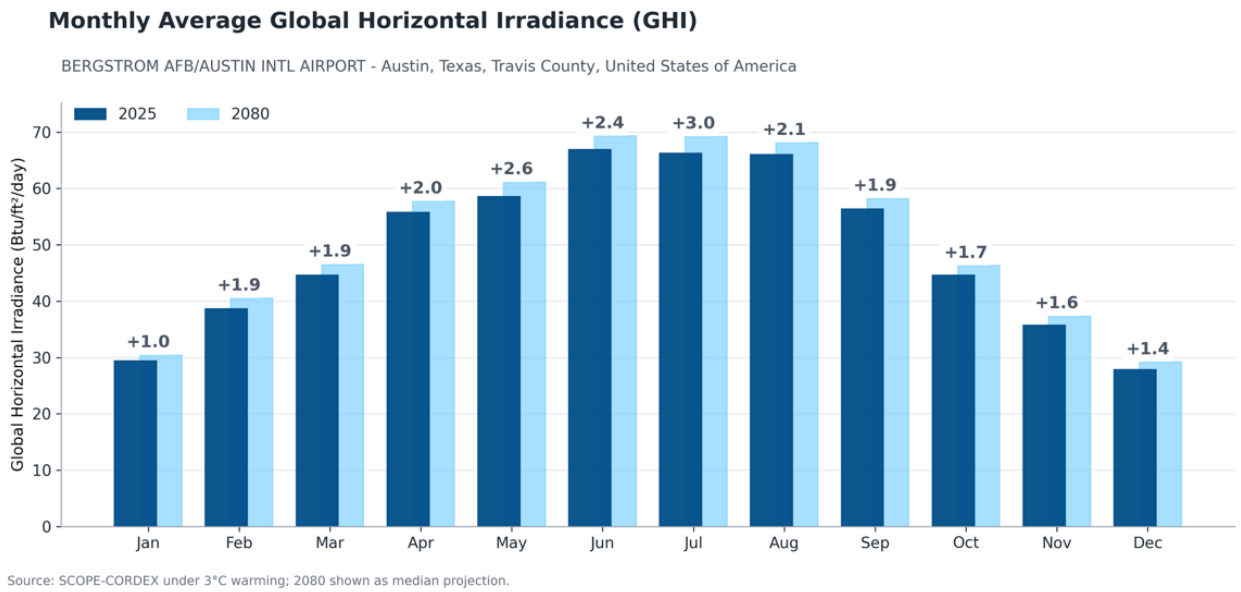

Figure 27 Projected monthly average global horizontal irradiance (GHI) at Austin–Bergstrom International Airport, comparing baseline (2025) and late-century (2080) conditions under approximately 3 °C of global mean warming.

Table 14 Projected monthly average global horizontal irradiance (Btu/ft²/day) at Austin–Bergstrom International Airport for baseline (2025), mid-century (2050), and late-century (2080) conditions. Values represent median projections, with ranges indicating the central model spread.

Btu/ft²/day	2025	2050	2080
January	29.4	29.8 (28.5-31.0)	30.4 (28.7-31.8)
February	38.6	39.6 (37.1-41.3)	40.5 (37.9-43.2)
March	44.6	45.6 (43.2-47.7)	46.5 (43.9-49.2)
April	55.7	56.8 (54.0-59.5)	57.7 (54.7-61.0)
May	58.5	60.0 (56.8-62.6)	61.1 (57.4-65.0)
June	66.9	68.2 (65.0-71.0)	69.3 (65.3-73.7)
July	66.2	67.7 (64.2-70.6)	69.2 (64.8-73.5)
August	66.0	66.9 (63.9-69.7)	68.1 (64.2-71.9)
September	56.3	57.3 (54.7-60.0)	58.2 (55.0-61.8)
October	44.6	45.5 (43.1-47.6)	46.3 (43.5-48.9)
November	35.7	36.5 (34.5-38.2)	37.3 (35.0-39.7)
December	27.8	28.4 (26.8-29.7)	29.2 (27.3-31.1)

7 Local Hazard Awareness

Secondary Hazard Overview - Travis County, TX

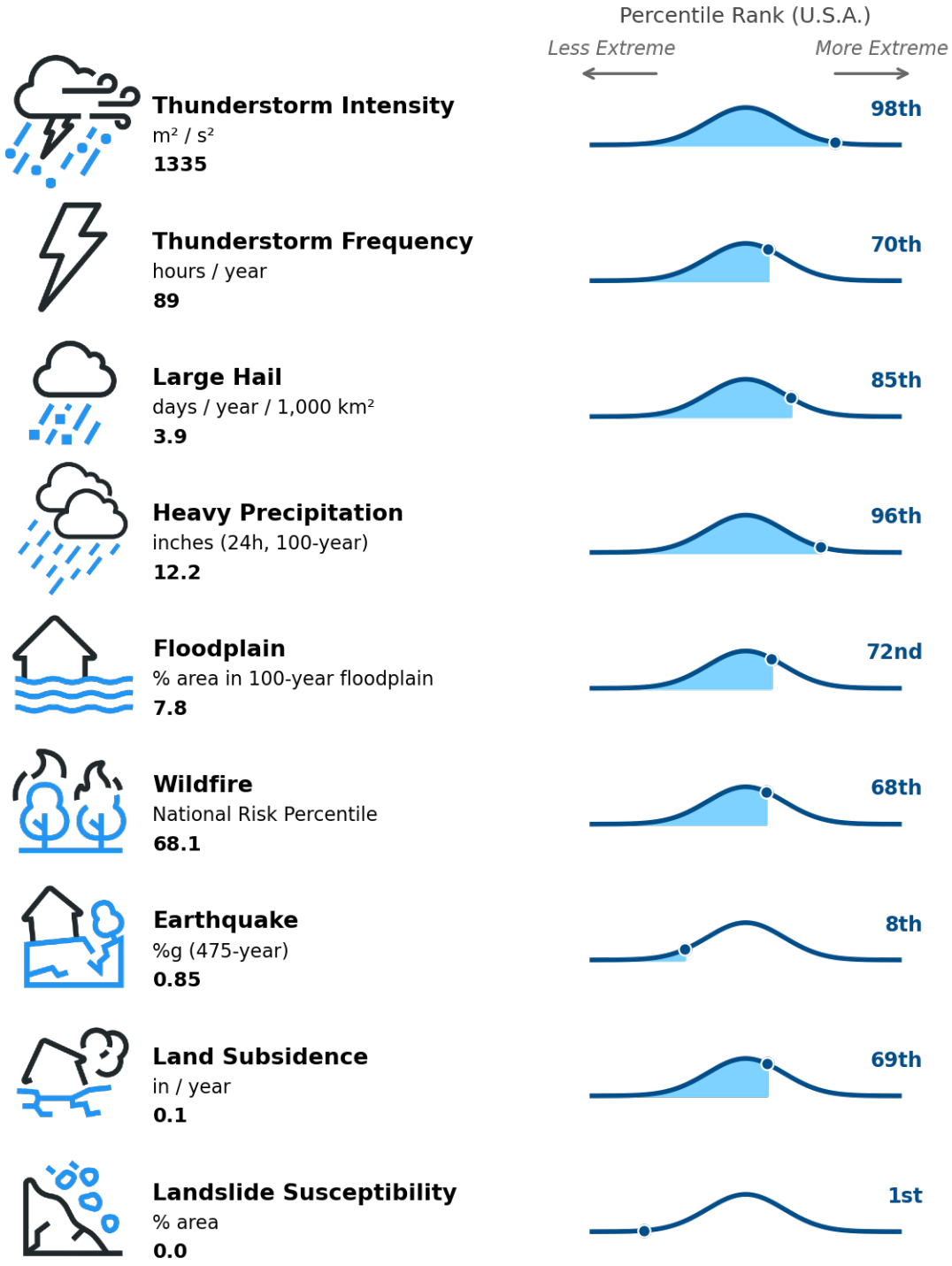

7.1 Landslide

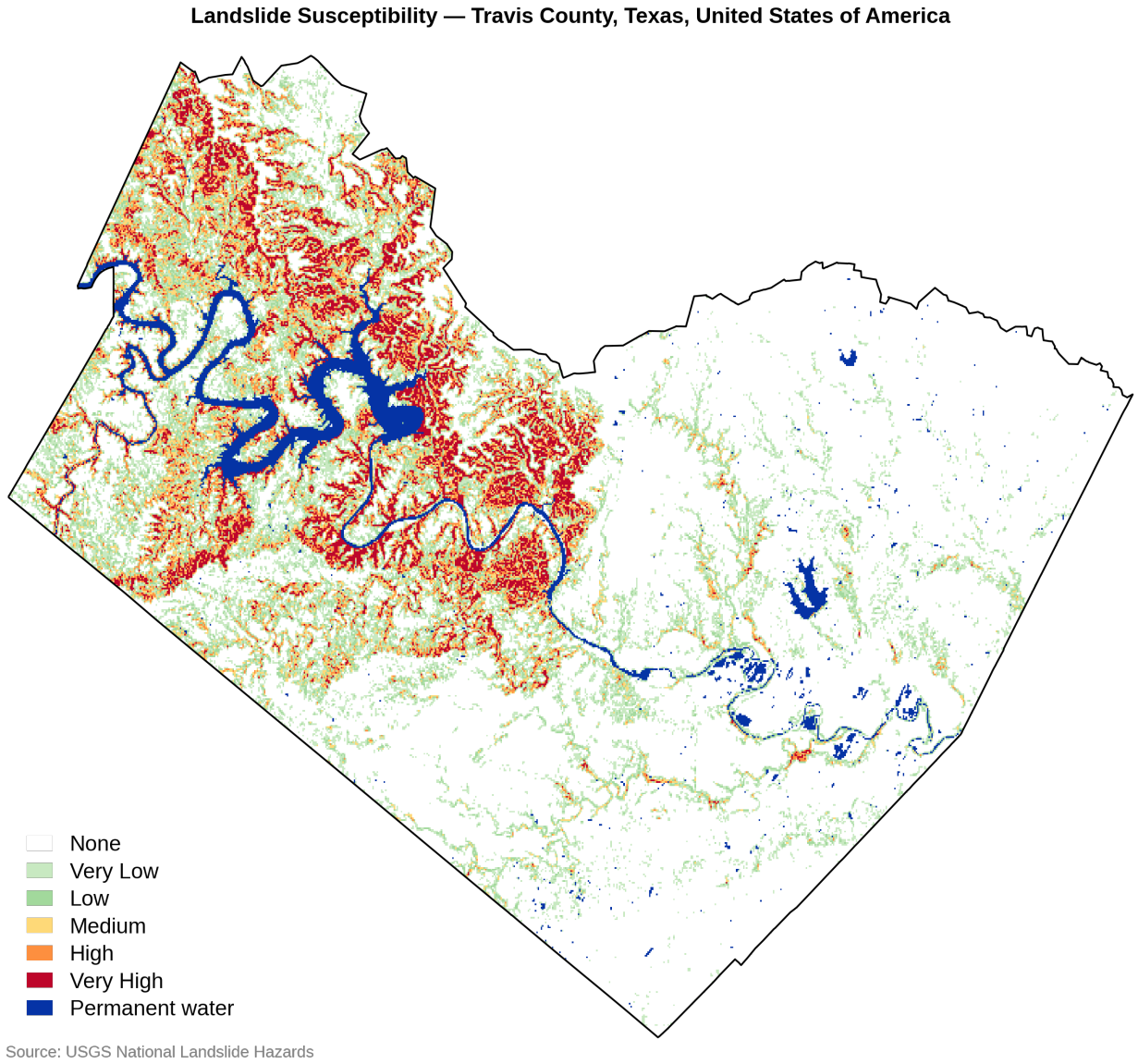

Figure 28 Landslide susceptibility across Travis County, Texas, showing relative likelihood categories from very low to very high based on terrain, geology, and hydrologic conditions. Map reflects baseline susceptibility from the USGS National Landslide Hazards dataset.

7.2 Flood

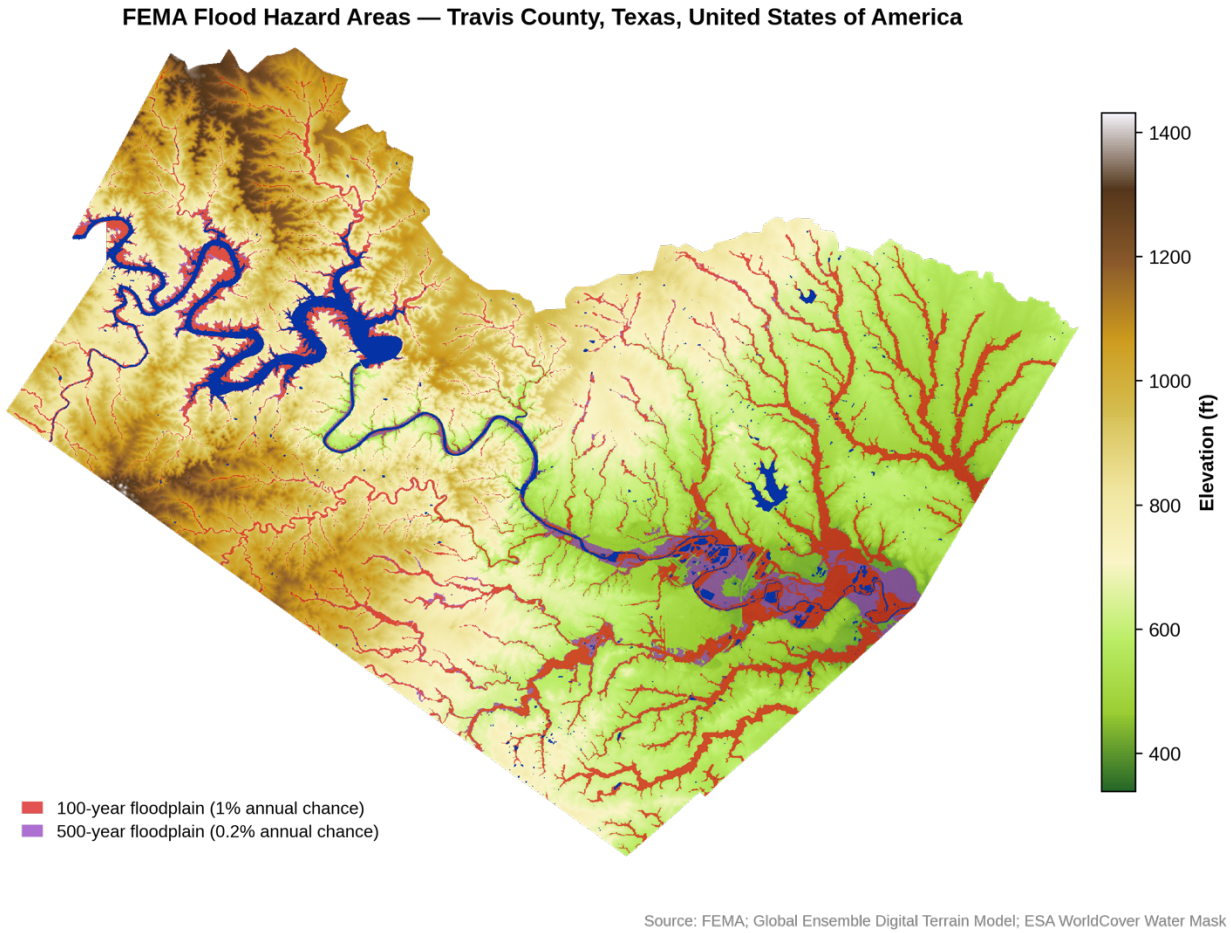

Figure 29 FEMA-designated flood hazard areas in Travis County, Texas, showing the 1% annual chance (100-year) and 0.2% annual chance (500-year) floodplains overlaid on local topography and surface water features. Flood extents are based on FEMA Flood Insurance Rate Maps.

7.3 Wildfire

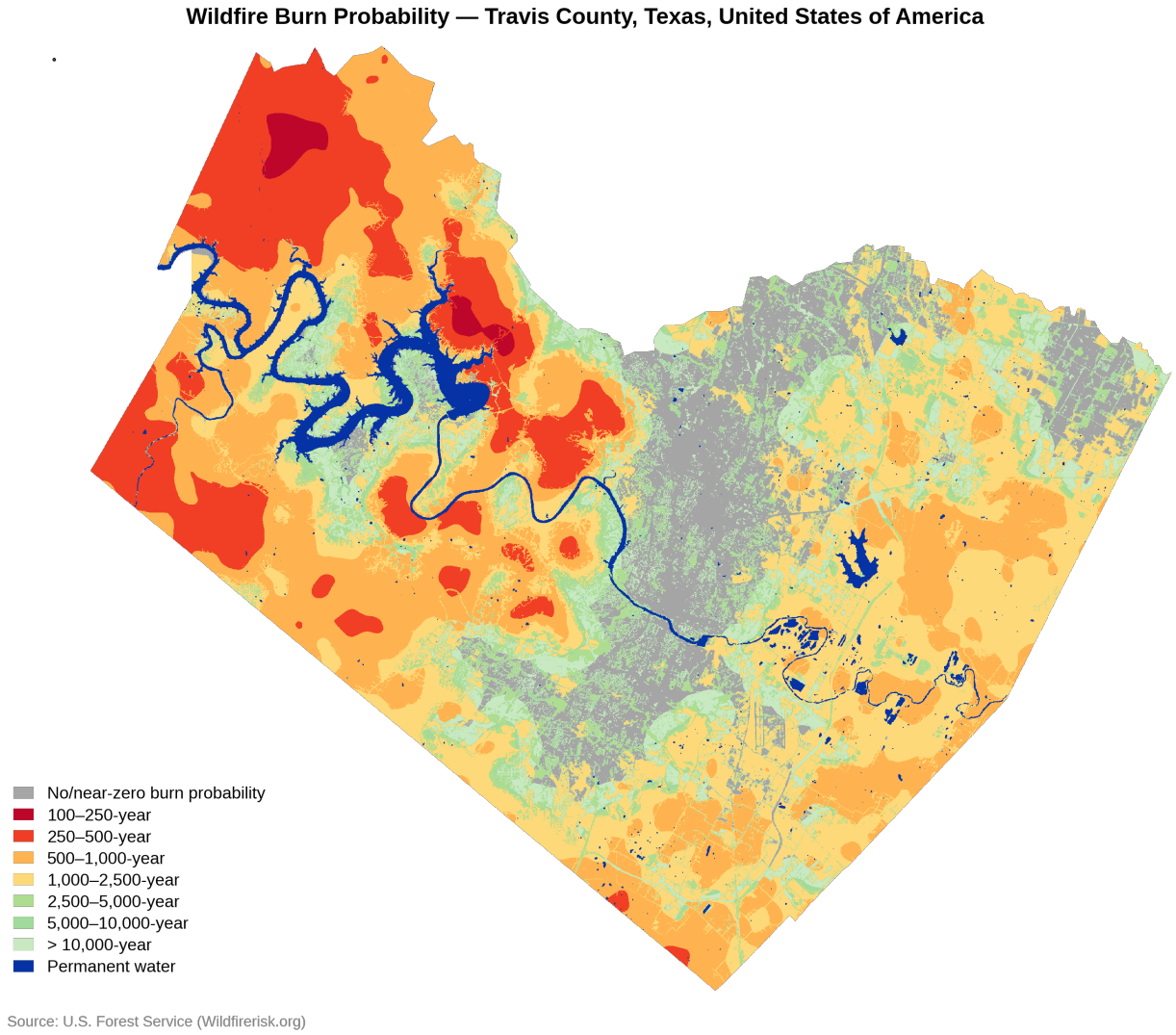

Figure 30 Wildfire burn probability across Travis County, Texas, expressed as approximate return-period classes based on historical fire occurrence and landscape characteristics. Map is derived from U.S. Forest Service wildfire risk products and represents baseline burn likelihood rather than climate-adjusted future wildfire risk.

APPENDIXES

Appendix A

Observational Data

Temperature, Humidity, and Wind

Climate design values are derived from the Hadley Centre Integrated Surface Dataset (HadISD), which provides quality-controlled hourly observations from a global network of surface weather stations, and the Global Historical Climatology Network–Daily (GHCN-Daily). Stations were selected using strict data completeness and quality criteria to ensure robust representation of local climate distributions and extremes. Observational records were gap-filled as needed, aggregated to daily values where applicable, and subjected to additional quality-control procedures following Rasmussen (2025).

Solar Radiation

Surface shortwave downwelling radiation (global horizontal irradiance, GHI) is derived from CHELSA-W5E5 v2.1, a globally consistent daily dataset at 30-arcsecond resolution (approximately 1 km at the equator) produced using orographic downscaling and climatological bias adjustment (Karger et al., 2023). Because no global, long-term, station-based archive of GHI exists, a gridded observation-calibrated product is required. CHELSA-W5E5 provides the spatial coverage and temporal consistency necessary for robust global analysis.

Extreme Precipitation

Extreme precipitation within the United States and its territories is characterized using NOAA Atlas 14, the authoritative source for precipitation frequency estimates in these regions. For locations outside the United States, rainfall depth return periods are estimated using a machine learning model trained on observed hourly and daily precipitation totals, as described in Hoch et al. (2025), to provide globally consistent frequency estimates where Atlas-style products are unavailable.

Extreme Wind Gusts

Within the United States, extreme 3-second gust wind speeds are based on the ASCE 7 Hazard Tool, which provides risk-targeted wind speed estimates consistent with ASCE/SEI 7 design standards. Outside the United States, extreme wind gusts are estimated by combining ERA5 hourly wind gust data for non-tropical cyclone conditions (1979–2023), downscaled to 1 km resolution, with synthetic tropical cyclone wind fields generated using the STORM (Synthetic Tropical cyclOne geneRation) model. STORM produces approximately 10,000 years of synthetic tropical cyclone tracks and associated wind fields, calibrated to historical observations from the IBTrACS database.

Climate Projections

Temperature, Humidity, Wind, and Solar Radiation.

Future temperature conditions are derived from SCOPE-CORDEX (Station-Calibrated Outputs for Planning & Engineering), a bias-adjusted dataset based on the CORDEX Grand Ensemble. SCOPE-CORDEX integrates high-resolution regional climate model projections (approximately 12.5–25 km) with quality-controlled station observations to generate location-specific temperature projections through 2100. In regions where CORDEX simulations are unavailable or limited, projections are supplemented using ISIMIP3b model outputs.

The SCOPE-CORDEX dataset applies Quantile Delta Mapping (QDM) bias adjustment (Cannon et al., 2015), which corrects historical distributional biases while preserving the projected climate change signal. The ensemble includes 184 unique GCM-RCM simulations across multiple emissions scenarios, providing robust representation of projection uncertainty.

Extreme Precipitation

Extreme precipitation projections utilize CMIP6 global climate models, comprising 28 unique global climate models (GCMs) with 1 to 7 ensemble members per model. These projections provide global coverage and represent the most recent generation of climate models, incorporating improved representations of physical processes compared to previous model generations.

Extreme Wind Gusts

Future projections of non-tropical cyclone (non-TC) wind gusts are based on daily mean wind speeds from four HighResMIP CMIP6 models simulated under the SSP5-8.5 scenario through 2050. Tropical cyclone (TC) wind gusts are derived using the synthetic tropical cyclone framework of Bloemendaal et al. (2022), which generates physically consistent TC wind fields calibrated to historical observations.

Additional Details Available:

Detailed information on data sources, model selection criteria, and processing workflows is provided in the supplemental methodology document available with purchased BuildForward™ reports.

Methodology

Temperature, Humidity, Wind, and Solar Radiation.

Historical Design Conditions Present-day design values were calculated from hourly observations over the most recent 25-year period using established statistical methods:

- Degree days computed from daily mean temperatures
- Annual percentile values (0.4%, 1%, 2%, 99%, 99.6%) derived from hourly frequency distributions
- Extreme value return levels (5, 10, 20, 50, 100-year) estimated using Generalized Extreme Value (GEV) distributions fitted via Bayesian methods, critical for assessing statistical uncertainty.

Climate Change Adjustment Future design conditions apply a delta change approach:

1. Calculate baseline values from climate model historical period (2005–2024)
2. Extract projected changes from climate models for each future decade
3. Add projected changes to observed baseline conditions

This method preserves the accuracy of observed data while incorporating physically consistent climate change signals from climate models across multiple variables.

Daily-to-Hourly Mapping (Temperature Variables) Because hourly climate model output is rarely available, an empirical transfer function maps daily climate projections to equivalent hourly design values. This approach leverages observed relationships between daily and hourly extremes at each station.

Extreme Precipitation

CMIP6 precipitation projections use a change factor approach, which assumes that systematic biases cancel out when calculating ratios between future and historical conditions. No bias adjustment is applied. Because extreme rainfall exhibits significant natural variability that can obscure climate trends, the multi-member ensemble structure (28 GCMs with 1 to 7 ensemble members each) is essential for isolating the climate change signal and characterizing projection uncertainty.

Extreme Wind Gusts

Annual maximum 3-second wind gusts are derived separately for tropical and non-tropical cyclone events: non-TC winds are extracted from ERA5 (with TC periods masked using IBTrACS dates), fitted with Gumbel distributions, and downscaled from 31 km to 1 km resolution using topographic predictors, while TC winds from STORM are converted from 10-minute averages to 3-second gusts and adjusted for local surface roughness using land-cover data. Future projections apply climate change signals from four HighResMIP CMIP6 models (SSP5-8.5, through 2050) directly to synthetic TC generation in STORM, while non-TC winds use a change factor approach based on projected changes in maximum daily wind speeds. The final hazard maps select the maximum value between TC and non-TC wind fields at each 1 km grid cell, with return periods ranging from 10 to 10,000 years covering global land areas and extending up to 50 km offshore.

Additional Details Available:

Complete technical specifications, including equations, statistical procedures, and validation results, are provided in the supplemental methodology document available with purchased BuildForward™ reports.

Projection Uncertainty

Warming Level Framework

Climate projection uncertainty is characterized using an ensemble approach across multiple models for a 3°C global warming level (2.5-3.8°C of warming above pre-industrial levels), rather than individual emissions scenarios. This framework facilitates risk assessment independent of specific policy pathways.

Traditional climate projections are organized by emissions scenarios (RCPs in CMIP5, SSPs in CMIP6, and future frameworks in CMIP7), which link climate outcomes to specific socioeconomic and policy assumptions about future greenhouse gas emissions. However, these scenarios introduce unnecessary complexity for infrastructure planning: a project designed for 3°C of warming will experience similar climate conditions regardless of whether that warming occurs in 2060 under a high-emissions pathway or 2080 under a moderate-emissions pathway with delayed mitigation.

By organizing projections around warming levels rather than emissions scenarios, we separate the physical climate response (what happens at 3°C) from the temporal question (when 3°C is reached). This approach recognizes that global mean temperature is the primary driver of regional climate change, and that models show strong agreement in regional responses at equivalent warming levels despite following different emissions trajectories to reach them. The framework remains valid across scenario frameworks (RCP, SSP, or future conventions), as it references the ultimate warming outcome rather than the emissions pathway that produces it.

This warming-based framework provides infrastructure designers and asset owners with climate conditions relevant to their planning horizons without requiring assumptions about future emissions policies, technological development, or socioeconomic trajectories that may unfold over the coming decades.

Model Ensemble Statistics

For each warming level, design conditions are summarized using the 5th, 50th (median), and 95th percentiles across the model ensemble. The median represents the central model tendency, while the 5th and 95th percentiles describe the central spread of model responses rather than absolute bounds.

The ensemble used here is an ensemble of opportunity, reflecting the available CORDEX and CMIP6 simulations rather than a purpose-built probabilistic ensemble. As a result, percentile ranges reflect both uncertainty in the modeled climate response and sampling limitations inherent in the existing model archive.

Return Period Uncertainty

Extreme value estimates (e.g., 100-year precipitation depths) carry additional statistical uncertainty from the limited length of observational records and the need to extrapolate beyond observed conditions. This uncertainty is quantified using confidence intervals derived from the fitted extreme value distributions, with wider intervals for rarer events. When combined with climate projection uncertainty, users receive both the model ensemble spread (capturing climate response uncertainty) and the statistical confidence bounds (capturing sampling uncertainty in the extreme value analysis).

References

Bloemendaal, N., Haigh, I. D., de Moel, H., Muis, S., Haarsma, R. J., & Aerts, J. C. J. H. (2020). Generation of a global synthetic tropical cyclone hazard dataset using STORM. Scientific Data, 7(1), 40. https://doi.org/10.1038/s41597-020-0381-2

Bloemendaal, N., de Moel, H., Martinez, A. B., Muis, S., Haigh, I. D., van der Wiel, K., Haarsma, R. J., van den Hurk, B. J. J. M., & Aerts, J. C. J. H. (2022). A globally consistent local-scale assessment of future tropical cyclone risk. Science Advances, 8(17), eabm8438. https://doi.org/10.1126/sciadv.abm8438

Cannon, A. J., Sobie, S. R., & Murdock, T. Q. (2015). Bias correction of GCM precipitation by quantile mapping: How well do methods preserve changes in quantiles and extremes? Journal of Climate, 28(17), 6938–6959. https://doi.org/10.1175/JCLI-D-14-00754.1

Coppola, E., et al. (2021). Twenty-first-century climate change in regional climate projections. Bulletin of the American Meteorological Society, 102(5), E1352–E1372. https://doi.org/10.1175/BAMS-D-20-0154.1

Dunn, R. J. H., Willett, K. M., Thorne, P. W., Woolley, E. V., Durre, I., Dai, A., Parker, D. E., & Vose, R. S. (2012). HadISD: A quality-controlled global synoptic report database for selected variables at long-term stations from 1973–2011. Climate of the Past, 8(5), 1649–1679. https://doi.org/10.5194/cp-8-1649-2012

Gutowski, W. J., Jr., et al. (2016). WCRP COordinated Regional Downscaling EXperiment (CORDEX): A diagnostic MIP for CMIP6. Geoscientific Model Development, 9(11), 4087–4095. https://doi.org/10.5194/gmd-9-4087-2016

Hoch, J. M., et al. (2025). BURGER: A bottom-up regionalization approach for global sub-daily intensity-duration-frequency data. Water Resources Research, 61(1), e2024WR039773. https://doi.org/10.1029/2024WR039773

Keune, J., Di Giuseppe, F., Barnard, C., et al. (2025). ERA5-Drought: Global drought indices based on ECMWF reanalysis. Scientific Data, 12, 616. https://doi.org/10.1038/s41597-025-04896-y

Rasmussen, D. J. (2025a). SCOPE-ERA5: Station-Calibrated Outputs for Planning & Engineering-ERA5. Zenodo. https://doi.org/10.5281/zenodo.15611602

Rasmussen, D. J. (2025b). Multivariate bias correction of ERA5 using in-situ observations for planning and engineering. ESS Open Archive. https://doi.org/10.22541/essoar.175130623.32640121/v1

Appendix B

Monthly Data Tables

Table 15 Monthly average daily maximum temperature (°F) at Austin–Bergstrom International Airport for baseline conditions (2025) and mid- and late-century periods (2050 and 2080). Values for 2050 and 2080 represent median projections, with ranges in parentheses indicating the central 90% of SCOPE-CORDEX model simulations corresponding to approximately 3 °C of global mean warming.

°F	2025	2050	2080
January	64.1	67.0 (64.6–70.3)	67.5 (63.9–69.6)
February	67.6	69.0 (67.8–71.6)	72.2 (68.9–75.4)
March	75.3	76.4 (73.9–78.3)	77.3 (74.0–80.5)
April	81.1	82.7 (80.4–84.7)	84.2 (83.0–86.7)
May	87.1	89.6 (88.1–92.4)	91.0 (89.2–93.8)
June	93.9	95.3 (93.4–97.0)	100.0 (97.0–103.4)
July	96	98.9 (96.4–100.5)	101.1 (97.0–102.6)
August	97.6	99.7 (96.5–101.0)	101.4 (99.0–102.6)
September	91.9	94.9 (91.7–96.5)	96.3 (92.4–97.8)
October	83.9	85.5 (82.8–87.2)	87.9 (84.5–91.1)
November	73.1	75.6 (71.8–78.1)	77.4 (73.9–79.1)
December	65.8	66.5 (64.3–71.2)	67.8 (64.9–70.6)

Table 16 Monthly average daily minimum temperature (°F) at Austin–Bergstrom International Airport for baseline conditions (2025) and mid- and late-century periods (2050 and 2080). Values for 2050 and 2080 represent median projections, with ranges in parentheses indicating the central 90% of SCOPE-CORDEX model simulations corresponding to approximately 3 °C of global mean warming.

°F	2025	2050	2080
January	39.9	44.3 (43.1–46.9)	45.5 (42.4–47.6)
February	43.8	46.6 (45.9–48.7)	50.0 (47.4–52.4)
March	51.8	52.6 (51.8–53.6)	54.5 (51.8–57.0)
April	58.1	60.1 (59.1–61.5)	59.7 (59.7–64.3)
May	66.2	69.4 (68.1–70.7)	70.6 (68.8–71.9)
June	72.6	74.0 (72.9–74.8)	75.8 (74.4–77.6)
July	73.9	76.2 (74.7–76.8)	78.4 (75.0–79.8)
August	74.4	76.6 (74.8–77.0)	78.4 (75.9–80.1)
September	69.2	71.9 (69.3–72.9)	74.0 (70.8–75.4)
October	58.8	60.2 (59.5–61.8)	63.2 (59.9–65.0)
November	49.5	53.9 (50.7–55.4)	54.5 (50.5–57.4)
December	42.9	43.4 (42.6–47.5)	46.3 (43.0–47.6)

Table 17 Annual and monthly total precipitation (inches) at Austin–Bergstrom International Airport for baseline conditions (2025) and mid- and late-century periods (2050 and 2080). Values for 2050 and 2080 represent median projections, with ranges in parentheses indicating the central 90% of CHELSA-CMIP6 model simulations corresponding to approximately 3 °C of global mean warming.

inches	2025	2050	2080
Annual	33.0	31.3 (29.0–36.2)	31.5 (30.2–33.7)
January	2.1	2.2 (2.0–2.4)	2.3 (1.8–2.5)
February	2.1	2.3 (1.9–2.5)	1.9 (1.8–2.2)
March	2.5	2.2 (2.0–3.1)	2.3 (2.1–2.7)
April	2.6	2.5 (2.3–3.4)	2.5 (2.1–3.7)
May	3.8	3.4 (2.9–4.4)	3.3 (3.1–3.7)
June	4.2	4.3 (3.4–4.9)	3.7 (3.4–4.1)
July	2.1	2.1 (1.9–2.5)	1.8 (1.7–2.2)
August	1.8	1.6 (1.3–1.7)	1.6 (1.3–1.8)
September	2.8	2.4 (2.1–3.2)	2.8 (2.2–3.6)
October	4.0	3.4 (2.7–4.2)	3.7 (3.2–4.4)
November	2.7	2.6 (2.4–3.0)	2.8 (2.4–3.2)
December	2.4	2.3 (2.1–2.8)	2.4 (2.1–2.8)

Table 18 Monthly mean wind speed (mph) at Austin–Bergstrom International Airport for baseline conditions (2025) and mid- and late-century periods (2050 and 2080). Values for 2050 and 2080 represent median projections, with ranges in parentheses indicating the central 90% of SCOPE-CORDEX model simulations corresponding to approximately 3 °C of global mean warming.

miles per hour	2025	2050	2080
January	8.1	7.5 (7.4–8.1)	8.1 (7.7–8.4)
February	9.2	8.9 (8.0–9.6)	9.1 (8.9–9.3)
March	9.4	9.7 (9.2–9.8)	9.4 (9.1–9.8)
April	9.4	9.6 (9.4–9.8)	9.5 (9.3–9.9)
May	9.0	9.8 (8.6–10.0)	9.5 (8.9–10.2)
June	8.4	9.1 (7.9–9.2)	9.3 (7.9–9.5)
July	7.7	7.9 (7.8–9.0)	8.5 (8.1–9.0)
August	7.3	6.9 (6.7–8.1)	7.2 (7.1–7.9)
September	6.5	6.8 (6.5–7.3)	6.4 (6.0–6.8)
October	7.1	7.4 (7.0–7.6)	7.0 (6.2–7.1)
November	7.5	7.8 (7.6–8.0)	7.5 (7.4–7.8)
December	7.6	7.7 (7.4–8.2)	7.8 (7.4–8.0)

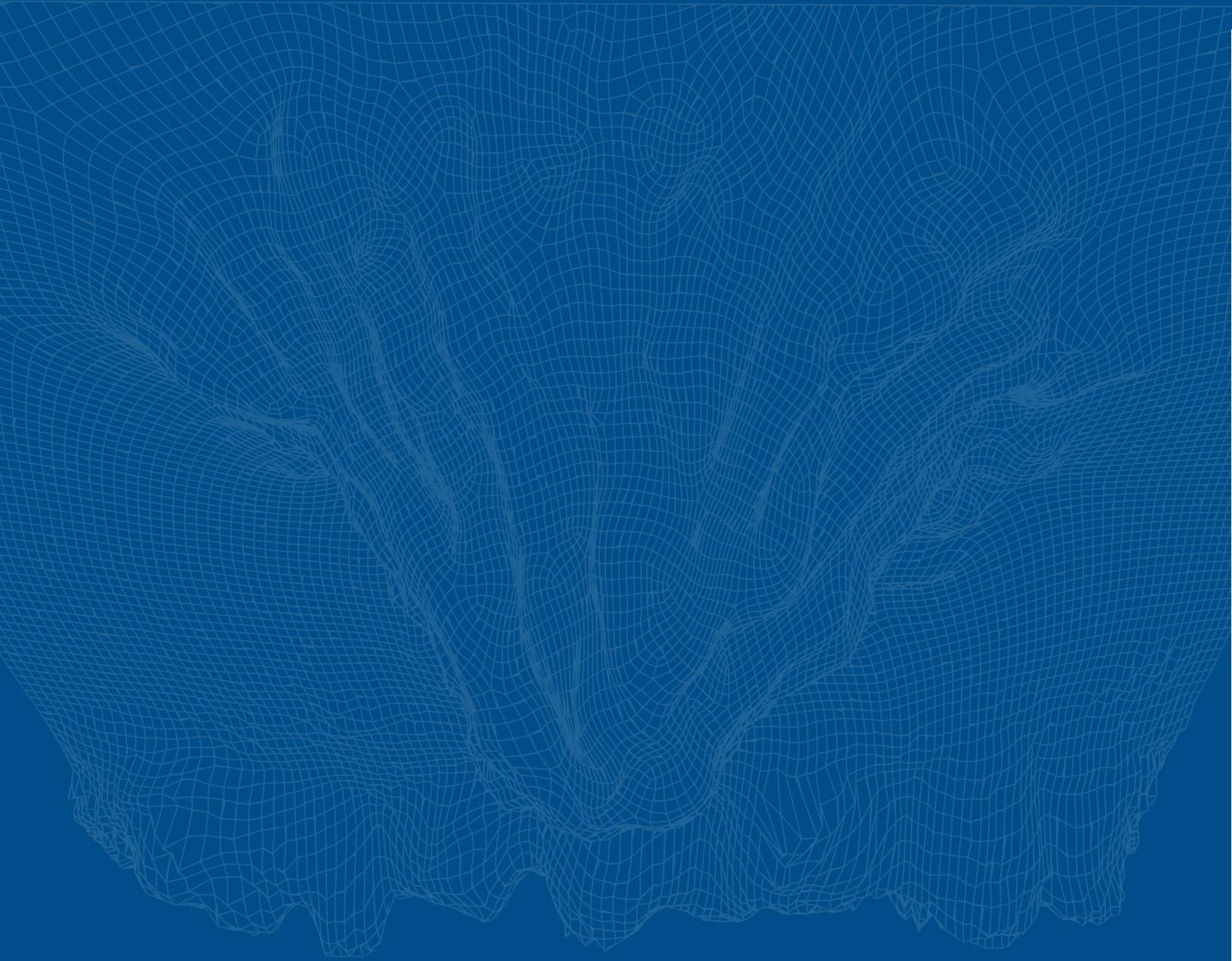

BuildForward™

buildforward.io
info@degreeday.org